Computer Assisted Mechanics and Engineering Sciences, 11: 293–320, 2004.

Coupling of FEM and EFGM with dynamic decomposition in 2D quasi-brittle crack growth analysis

Jan Jaśkowiec and Czesław Cichoń
Institute of Computer Methods in Civil Engineering, Cracow University of Technology, ul. Warszawska 24, 31-155 Kraków, Poland

(Received April 8, 2003)

In the paper three computational models for crack growth analysis in quasi-brittle materials in plane stress state are presented. These models have been worked out on the base of different methods of coupling the finite element method and the element free Galerkin method. Effectiveness of the methods of analysis are improved by the algorithm of dynamic domain decomposition into Ω^h, Ω^ϱ, $\Omega^{h\varrho}$ parts. The usefulness of the methods in crack growth analysis has been confirmed in examples.

1. Introduction

Finite element method (FEM) is a widely accepted and trusted method of numerical analysis in solid mechanics. The basic ideas of FEM are discretisation of the domain solution by finite elements and approximation of unknown functions in elements [24]. A different approach where approximation is based on nodes rather than finite elements is used in the group of methods known as the meshless methods [15]. Among the meshless methods the element free Galerkin method (EFGM) is most often applied to the analysis of solid mechanics problems and in the paper the method is utilized.

The coupling of FE and EFG methods seems to be attractive in finding approximated solutions of engineering problems. Such approach applies advantages of both methods and hides their drawbacks at the same time. As it is stated in [12], EFGM does not require generation a connectivity matrix and is specially suited for problems like adaptive refinement computations, problems with high gradients, concentrated forces, large deformations or crack propagation analysis. FEM is, on the other hand, less costly, Dirichlet boundary conditions are applied in a simple way and is widely accepted by engineers.

EFGM usually gives better results than FEM when the same number of degrees of freedom is used, however, since EFGM is much more costly, therefore the coupling algorithm should work in such a way that EFGM is applied to specific, relatively small areas of solution domain Ω where FEM does not work well.

The basic equations of FEM and EFGM are shortly described in Sec. 2 with special attention to the definition of approximation fields. In the paper the Partition of Unity Method (PUM) is utilized and also is shortly described in Sec. 2.

In Sec. 3 three methods of coupling FEM and EFGM are formulated which are based on the algorithm presented in [12]. Additionally, the fourth coupling method is formulated with the help of PUM.

To couple the two methods the domain of solution Ω has to be partitioned into three parts: (i) Ω^h – the finite element part, (ii) Ω^ϱ – the meshless part and (iii) $\Omega^{h\varrho}$ – the region where Ω^h and Ω^ϱ overlap. In order to improve the effectiveness of the coupling method in the crack growth analysis in Sec. 3 an algorithm for the dynamic domain decomposition is proposed.

The coupling methods are used in Sec. 4 to elaborate three computational models for crack growth analysis: (i) standard model, (ii) enriched base model and (iii) partition of unity model. The

quasi-brittle material is assumed and therefore the fictitious crack model is used for crack growth description. In Sec. 4 the iteration method of solution of an incremental set of equations of the crack growth problem is also presented.

The correctness of the proposed coupling methods with dynamic decomposition, consequently computational models, is illustrated with three examples in Sec. 5. The first example is the Laplace problem and the other two examples concern crack propagation analysis. The paper ends with some conclusions.

2. FEM and EFGM formulations

2.1. Problem formulation

The problems considered in the paper can be formulated as follow:

Find the function $u \in \mathcal{V} \subset H$ such that variational equation

$$a(u,v) = l(v)\,, \qquad \forall v \in \mathcal{V}_o\,, \tag{1}$$

is fulfilled where $a(\cdot,\cdot)$ is a symmetric and positive–defined bilinear form and $l(\cdot)$ is a linear form, v is a test function that satisfies the essential boundary conditions and $\mathcal{V}$ is a subspace of the Sobolev space H and $\mathcal{V}_o \subset \mathcal{V}$.

An approximated solution of the problem (1) in finite-dimensional subspace $\widetilde{\mathcal{V}} \subset \mathcal{V}$ is the function $\tilde{u} \in \widetilde{\mathcal{V}}$, such that equation

$$a(\tilde{u},\tilde{v}) = l(\tilde{v})\,, \qquad \forall \tilde{v} \in \widetilde{\mathcal{V}}_o\,, \tag{2}$$

is fulfilled where $\widetilde{\mathcal{V}}_o \subset \widetilde{\mathcal{V}}$.

The solution of Eq. (2) can be obtained using different computer methods. In the case of finite element method the subspace $\widetilde{\mathcal{V}} = \text{ span}\{N_i^h\}$, where $i \in I^h$, and in the case of free Galerkin method, the subspace $\widetilde{\mathcal{V}} = \text{ span}\{N_i^\varrho\}$ where $i \in I^\varrho$. It means that one of the basic differences between FE and EFG methods lies in the definition of approximation functions $N_i^k(\mathbf{x})$, $k = h, \varrho$. This simple statement will be used to define various coupled FE-EFG methods. At first, however, the methods which are used in the paper will be shortly described and details connected with approximation fields will be emphasized.

2.2. Finite Element Method (FEM)

According to the procedure of the finite element method the solution domain Ω is divided into a finite number E of elements Ω_e, $\Omega \approx \Omega^h = \bigcup_{e=1}^{E} \Omega_e$.

Unknown function $u(\mathbf{x})$ can be approximated by function $\mathcal{A}^h u(\mathbf{x})$ in the element Ω_e using formula

$$u(\mathbf{x}) \approx \mathcal{A}^h u(\mathbf{x}) = \sum_{i \in I_e^h} p_i^h(\mathbf{x})\, a_i^e = \left(\mathbf{p}^h(\mathbf{x})\right)^{\mathrm{T}} \mathbf{a}^e\,, \qquad \forall \mathbf{x} \in \Omega_e\,, \tag{3}$$

where $\mathbf{x}$ is the global coordinate system, $\left\{p_i^h(\mathbf{x})\right\}_{i \in I_e^h}$ is a set of complete base functions, $\left\{a_i^e\right\}_{i \in I_e^h}$ are mathematical degrees of freedom and I_e^h is a set of global node numbers for element Ω_e.

Approximation (3) can also be expressed with the help of element shape functions $N_i^e(\mathbf{x})$

$$\mathcal{A}^h u(\mathbf{x}) = \sum_{i \in I_e^h} N_i^e(\mathbf{x})\, u_i\,, \qquad \forall \mathbf{x} \in \Omega_e\,, \tag{4}$$

where u_i are values of $u(\mathbf{x})$ at the preselected nodes $\mathbf{x}_i$ (global degrees of freedom).

Now we introduce the definition of global interpolation functions in the domain Ω^h in the form

$$N_i^h(\mathbf{x}) = \begin{cases} 0 & \text{when } \mathbf{x} \in \Omega_e \text{ and } i \notin I_e^h, \\ N_i^e(\mathbf{x}) & \text{when } \mathbf{x} \in \Omega_e \text{ and } i \in I_e^h. \end{cases} \tag{5}$$

In the following functions $N_i^h(\mathbf{x})$ are called global finite element (GFE) shape functions (also called global interpolation functions [18]).

Interpolant of function $u(\mathbf{x})$ can then be written by a linear combination of the form

$$\mathcal{A}^h u(\mathbf{x}) = \sum_{i \in I^h} N_i^h(\mathbf{x})\, u_i\,, \qquad \forall \mathbf{x} \in \Omega^h\,, \tag{6}$$

where $I^h = \bigcup_{e=1}^{E} I_e^h$.

The finite element method can be defined with the help of *GFE shape functions* $N_i^h(\mathbf{x})$ in the following way.

Definition 1. *Finite element method*

Let $\mathcal{V}^h := \operatorname{span}\{N_i^h\}$. *Find the function* $u^h \in \mathcal{V}^h$ *that fulfills the equation*

$$a(u^h, v^h) = l(v^h)\,, \qquad \forall\, v^h \in \mathcal{V}_o^h\,, \tag{7}$$

with the essential boundary conditions.

2.3. Element Free Galerkin method (EFGM)

2.3.1. EFGM shape functions

Let us assume that function $u(\mathbf{x})$, defined on a domain Ω, is approximated by function $\mathcal{A}^\varrho u(\mathbf{x})$ given by

$$u(\mathbf{x}) \approx \mathcal{A}^\varrho u(\mathbf{x}) = \mathbf{p}^{\varrho\mathrm{T}}(\mathbf{x})\,\mathbf{a}(\mathbf{x})\,, \qquad \forall \mathbf{x} \in \Omega\,, \tag{8}$$

where $\{p_i(\mathbf{x})\}_{i=1,2,\ldots,L}$, $\{a_i(\mathbf{x})\}_{i=1,2,\ldots,L}$ are vectors of base functions and vector of unknown coefficients, respectively, and L is the number of base functions.

The above approximation formula can also be written in the form of a linear combination of functions $N_j^\varrho(\mathbf{x})$ and nodal values of approximated function $u_j = u(\mathbf{x}_j)$

$$\mathcal{A}^\varrho u(\mathbf{x}) = \sum_{j \in I^\varrho} N_j^\varrho(\mathbf{x})\, u_j\,, \qquad \forall \mathbf{x} \in \Omega\,, \tag{9}$$

where I^ϱ is a set of global node numbers in the domain Ω. In analogy to the definition of shape functions introduced in point 2.2, the approximation functions $N_i^\varrho(\mathbf{x})$ are called EFG shape functions [1]. EFG shape functions can be determined imposing the so-called consistency condition which is of the form

$$\mathbf{p}^\varrho(\mathbf{x}) = \sum_{j \in I^\varrho} \mathbf{p}^\varrho(\mathbf{x}_j)\, N_j^\varrho(\mathbf{x})\,. \tag{10}$$

In the context of weighted moving least square (WMLS) approximation, the shape functions can be expressed as [12]

$$N_j^\varrho(\mathbf{x}) = \mathbf{p}^{\varrho\mathrm{T}}(\mathbf{x}_j)\,\boldsymbol{\alpha}(\mathbf{x})\, w(r_j)\,, \tag{11}$$

where $\boldsymbol{\alpha}(\mathbf{x})$ is the unknown vector and $w(r_j)$ is the weight function and $r_j = \|\mathbf{x} - \mathbf{x}_j\|$. It is assumed that the weight function $w(r)$ is symmetric and has compact support which also describes the support of EFG shape functions.

After substitution of Eq. (11) into Eq. (10) the linear system of equations that determines $\boldsymbol{\alpha}(\mathbf{x})$ is obtained

$$\mathbf{M}(\mathbf{x})\,\boldsymbol{\alpha}(\mathbf{x}) = \mathbf{p}^{\varrho}(\mathbf{x})\,, \tag{12}$$

with

$$\mathbf{M}(\mathbf{x}) = \sum_{j \in I^{\varrho}} \mathbf{p}^{\varrho}(\mathbf{x}_j)\,\mathbf{p}^{\varrho \mathrm{T}}(\mathbf{x}_j)\,w(r_j)\,.$$

The final formula for calculation of the shape function $N_j^{\varrho}(\mathbf{x})$ formally has the form

$$N_j^{\varrho}(\mathbf{x}) = \mathbf{p}^{\varrho \mathrm{T}}(\mathbf{x}_j)\left(\mathbf{M}(\mathbf{x})\right)^{-1}\mathbf{p}^{\varrho}(\mathbf{x})\,w(r_j)\,. \tag{13}$$

The derivative of EFG shape function is calculated using formula

$$N_{j,x}^{\varrho}(\mathbf{x}) = \mathbf{p}^{\varrho \mathrm{T}}(\mathbf{x}_j)\,\boldsymbol{\alpha}_{,x}(\mathbf{x})\,w(r_j) + \mathbf{p}^{\varrho \mathrm{T}}(\mathbf{x}_j)\,\boldsymbol{\alpha}(\mathbf{x})\,w_{,x}(r_j)\,. \tag{14}$$

In the above expression the derivative of $\boldsymbol{\alpha}(\mathbf{x})$ has appeared and can be easily obtained by differentiation of Eq. (11)

$$\mathbf{M}(\mathbf{x})\,\boldsymbol{\alpha}_{,x}(\mathbf{x}) + \mathbf{M}_{,x}(\mathbf{x})\,\boldsymbol{\alpha}(\mathbf{x}) = \mathbf{p}^{\varrho}{}_{,x}(\mathbf{x})\,, \tag{15}$$

where

$$\mathbf{M}_{,x}(\mathbf{x}) = \sum_{j=1}^{J} \mathbf{p}^{\varrho}(\mathbf{x}_j)\,\mathbf{p}^{\varrho \mathrm{T}}(\mathbf{x}_j)\,w_{,x}(r_j)\,.$$

Solving Eq. (15) for $\boldsymbol{\alpha}_{,x}(\mathbf{x})$ the following formula is obtained

$$\boldsymbol{\alpha}_{,x}(\mathbf{x}) = \left(\mathbf{M}(\mathbf{x})\right)^{-1}\left(\mathbf{p}^{\varrho}{}_{,x}(\mathbf{x}) - \mathbf{M}_{,x}(\mathbf{x})\,\boldsymbol{\alpha}(\mathbf{x})\right). \tag{16}$$

The base functions in vector $\mathbf{p}^{\varrho}(\mathbf{x})$ generally can be quite arbitrary. In most cases, however, the functions are polynomial. In some cases the character of exact solution is known a priori, then some special functions can be included in the approximation. When EFGM is enriched with special functions then in the paper it is named enriched EFGM (EFGME).

The element free Galerkin method can now be defined with the help of EFG shape functions $N_j^{\varrho}(\mathbf{x})$ in the following way.

Definition 2. *Element free Galerkin method*

Let $\mathcal{V}^{\varrho} := \operatorname{span}\{N_j^{\varrho}\}$. *Find the function* $u^{\varrho} \in \mathcal{V}^{\varrho}$ *that fulfils the equation*

$$a(u^{\varrho}, v^{\varrho}) = l(v^{\varrho})\,, \quad \forall\, v^{\varrho} \in \mathcal{V}_o^{\varrho}\,, \tag{17}$$

with the essential boundary conditions.

2.4. Partition of Unity (PU)

In the paper to enrich approximation the partition of unity method is also used [9, 16]. In that case the approximation functions are expressed by the formula

$$\phi_{ik}(\mathbf{x}) = \varphi_i^m(\mathbf{x})\,\gamma_k(\mathbf{x})\,, \tag{18}$$

where $\{\varphi_i^m(\mathbf{x})\}$ is a set of functions with completeness of order m and $\gamma_k(\mathbf{x})$ are assumed to be enriching functions and $k = 1, \ldots, K$, K is the number of enriching functions.

Functions $\varphi_i^m(\mathbf{x})$ fulfil conditions

$$\sum_{i=1}^{I} \varphi_i^m(\mathbf{x}) = 1\,, \qquad \Omega \subset \bigcup_{i=1}^{I} \operatorname{supp}\{\varphi_\alpha^m\}\,, \tag{19}$$

where I is the number of nodes.

From the above equations the following equality can be written

$$\sum_{i=1}^{I} \phi_{ik} = \gamma_k\,, \tag{20}$$

which means that functions $\gamma_k(\mathbf{x})$ can be recovered exactly by $\phi_{ik}(\mathbf{x})$.

Function $u(\mathbf{x})$ can be approximated with the formula

$$u(\mathbf{x}) \approx \sum_{i=1}^{I}\sum_{k=1}^{K} \phi_{ik} b_{ik}\,, \tag{21}$$

where b_{ik} are approximation coefficients.

Functions $\varphi_i^m(\mathbf{x})$ can be formulated in a different way. In the paper it is assumed that $\varphi_i^m(\mathbf{x}) = N_i(\mathbf{x})$, where $N_i(\mathbf{x})$ are GFE shape functions, EFG shape functions or their combinations.

If PU method is applied only to some subdomain, then the approximation takes the form

$$u(\mathbf{x}) = \sum_{i=1}^{I} N_i(\mathbf{x})\, a_i + \sum_{i=1}^{I}\sum_{k=1}^{K} N_i(\mathbf{x})\,\gamma_k(\mathbf{x})\,\mathcal{B}\, b_{ik}\,, \tag{22}$$

which is the sum of standard and enriching part of approximation, where $\mathcal{B}$ is Boolean matrix, a_i are standard degrees of freedom and b_{ik} are now additional degrees of freedom. If $N_i(\mathbf{x})$ are GFE shape functions then approximation (22) is a base for formulation of the so-called extended FEM (XFEM). By analogy, in Eq. (22) $N_i(\mathbf{x})$ are EFG shape functions, when the method is called the extended EFG method (XEFGM).

2.5. Integration

The solution of Eq. (7) or (17) needs numerical integration to be performed. It can be said in general that in case of FEM the numerical integration is carried out in integration cells, which are finite elements. In EFGM, however, integration cells have to be additionaly introduced. Integration in EFGM is troublesome since the EFG shape functions are not polynomials and their supports generally have spherical shapes. In consequence, the support border of EFG shape functions always goes through integration cells, Fig. 1.

In the paper, the mesh of integration cells in EFGM is composed using any finite element mesh generator. In such a way the mesh of basic cells is described. Then each basic cell is divided into integration cells, where the proper quadrature is applied, Fig. 2. Such approach showed to be especially effective in the process of coupling FE and EFG methods.

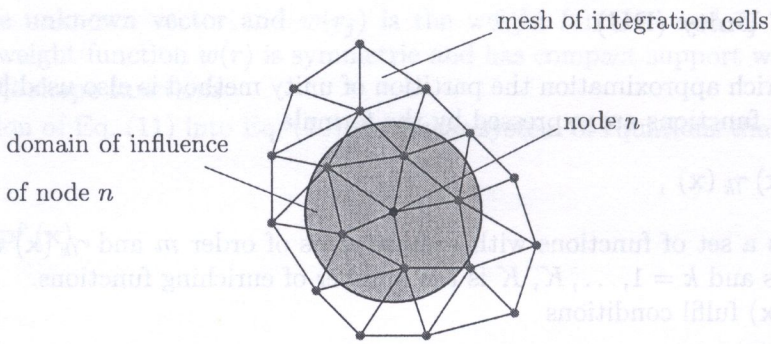

Fig. 1. Domain of influence for node and mesh of integration cells

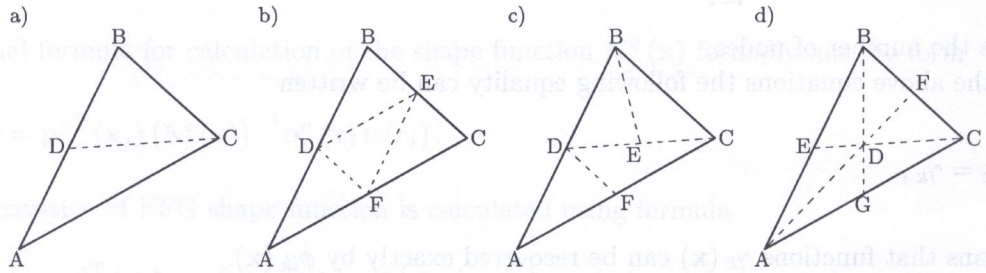

Fig. 2. Triangle partition scheme into two, four and six integration cells

3. Coupling of FE and EFG methods

3.1. Methods of coupling

Let us assume that the domain of solution Ω is partitioned into parts: (i) Ω^h – the FEM part, (ii) Ω^ϱ – the EFGM part ($\Omega^h \bigcup \Omega^\varrho \subset \Omega$), (iii) $\Omega^{h\varrho}$ – the region where Ω^h and Ω^ϱ overlap each other ($\Omega^{h\varrho} = \Omega^h \bigcap \Omega^\varrho$).

The parts Ω^h and Ω^ϱ fulfil the following relations

$$\begin{aligned} \Omega^h &= \left\{x \in \Omega \,|\, \exists i \in I^h \quad N_i^h(\mathbf{x}) \neq 0\right\}, \\ \Omega^\varrho &= \left\{x \in \Omega \,|\, \exists j \in I^\varrho \quad N_j^\varrho(\mathbf{x}) \neq 0\right\}. \end{aligned} \tag{23}$$

In the paper three coupling methods are formulated:

1. FEM-EFGM – in this method the same polynomial base functions are used in approximation in Ω^h and Ω^ϱ, Fig. 3a.

2. FEM-EFGME – it means that approximation in Ω^ϱ is enriched with special functions, Fig. 3a.

3. EFEM-EFGM – in this method FEM approximation is enriched in $\Omega^{h\varrho}$ part by shape functions of enriched EFG method, Fig. 3b.

In Sec. 4 the above coupling methods are used to introduce computational models for crack growth analysis. The first method is used in point 4.3 to formulate the standard computational model and two following methods are used in point 4.4. to formulate the enriched based computational model. In point 4.5 the third computational model, called the partition of unity computational model, is presented where the FEM-XEFGM coupling method is applied. It is based on the FEM-EFGM coupling where, however, in the domain Ω^ϱ approximation field is enriched with the help of Eq. (22), Fig. 3c.

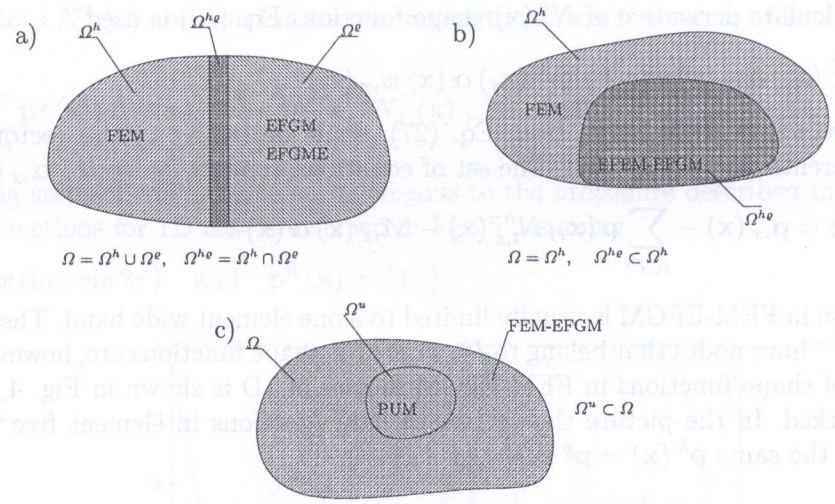

Fig. 3. Partition of solution domain: a) FEM-EFGM & FEM-EFGME, b) EFEM-EFGM, c) FEM-XEFGM

3.2. FEM-EFGM coupling

The approximation in Ω^{he} is constructed as a superposition of finite element interpolation and element free approximation [12]

$$\mathcal{A}^{ue}u(\mathbf{x}) = \sum_{i\in I^h} N_i^h(\mathbf{x})\, u(\mathbf{x}_i) + \sum_{j\in I^e} N_j^e(\mathbf{x})\, u(\mathbf{x}_j)\,, \qquad \forall \mathbf{x}\in\Omega^{he}\,. \tag{24}$$

The finite element shape functions $N_i^h(\mathbf{x})$ are supposed to be known, while the element free shape functions $N_j^e(\mathbf{x})$ are not known and will be evaluated using consistency condition.

In the method the order of completeness of approximation fields of EFG and FE methods is the same. If we assume that $\mathbf{p}(\mathbf{x}) = \mathbf{p}^h(\mathbf{x}) = \mathbf{p}^e(\mathbf{x})$ then the following relation is true

$$\begin{aligned} &\sum_{i\in I^h} \mathbf{p}(\mathbf{x}_i)\, N_i^h(\mathbf{x}) = \mathbf{p}(\mathbf{x})\,, \qquad \forall \mathbf{x}\in\Omega^h\backslash\Omega^{he} \\ &\Leftrightarrow \\ &\sum_{i\in I^e} \mathbf{p}(\mathbf{x}_i)\, N_i^e(\mathbf{x}) = \mathbf{p}(\mathbf{x})\,, \qquad \forall \mathbf{x}\in\Omega^e\backslash\Omega^{he}\,. \end{aligned} \tag{25}$$

The finite element shape functions are not complete in the Ω^{he} part, which means that they are not defined for nodes on the boundary Ω^{he} and $\Omega^e \setminus \Omega^{he}$. The completeness has been recovered with the help of $N_i^e(\mathbf{x})$ shape functions.

The consistency condition of the mixed approximation in Ω^{he} takes the form

$$\mathbf{p}(\mathbf{x}) = \sum_{i\in I^h} \mathbf{p}(\mathbf{x}_i)\, N_i^h(\mathbf{x}) + \sum_{j\in I^e} \mathbf{p}(\mathbf{x}_j)\, N_j^e(\mathbf{x})\,, \qquad \forall \mathbf{x}\in\Omega^{he}\,. \tag{26}$$

The $N_j^e(\mathbf{x})$ shape functions are expressed using Eq. (11). After substitution of Eq. (11) into Eq. (26) the linear system of equations that determines $\boldsymbol{\alpha}(\mathbf{x})$ is obtained

$$\mathbf{M}(\mathbf{x})\,\boldsymbol{\alpha}(\mathbf{x}) = \mathbf{p}(\mathbf{x}) - \sum_{i\in I^h} \mathbf{p}(\mathbf{x}_i)\, N_i^h(\mathbf{x})\,. \tag{27}$$

Eventually the formula for calculation of EFG shape functions in Ω^{he} has the form

$$N_j^e(\mathbf{x}) = \mathbf{p}^{\mathrm{T}}(\mathbf{x}_j)\left(\mathbf{M}(\mathbf{x})\right)^{-1}\Big(\mathbf{p}(\mathbf{x}) - \sum_{i\in I^h} \mathbf{p}(\mathbf{x}_i)\, N_i^h(\mathbf{x})\Big) w(r_j)\,. \tag{28}$$

In order to calculate derivative of $N_j^{\varrho}(\mathbf{x})$ shape functions Eq. (10) is used

$$N_{j,x}^{\varrho}(\mathbf{x}) = \mathbf{p}^{\mathrm{T}}(\mathbf{x}_j)\,\boldsymbol{\alpha}_{,x}(\mathbf{x})\,w(r_j) + \mathbf{p}^{\mathrm{T}}(\mathbf{x}_j)\,\boldsymbol{\alpha}(\mathbf{x})\,w_{,x}(r_j)\,. \tag{29}$$

In Eq. (29) vector $\boldsymbol{\alpha}(\mathbf{x})$ is taken from Eq. (27), while derivative of the vector can easily be obtained by differentiation of Eq. (26). The set of equations appears for vector $\boldsymbol{\alpha}_{,x}(\mathbf{x})$ in the form

$$\mathbf{M}(\mathbf{x})\,\boldsymbol{\alpha}_{,x}(\mathbf{x}) = \mathbf{p}_{,x}(\mathbf{x}) - \sum_{i\in I^h} \mathbf{p}(\mathbf{x}_i)\,N_{i,x}^{h}(\mathbf{x}) - \mathbf{M}_{,x}(\mathbf{x})\,\boldsymbol{\alpha}(\mathbf{x})\,. \tag{30}$$

The $\Omega^{h\varrho}$ region in FEM-EFGM is usually limited to a one element wide band. The finite elements that belong to $\Omega^{h\varrho}$ have nodes that belong to I^{ϱ}, where FE shape functions are, however, incomplete.

An example of shape functions in FEM-EFGM in case of 1D is shown in Fig. 4, where Ω^{ϱ}, Ω^{h} and $\Omega^{h\varrho}$ are marked. In the picture the vectors of base functions in element free part and finite element part are the same $\mathbf{p}^h(\mathbf{x}) = \mathbf{p}^{\varrho}(\mathbf{x}) = \{1 \quad x\}$.

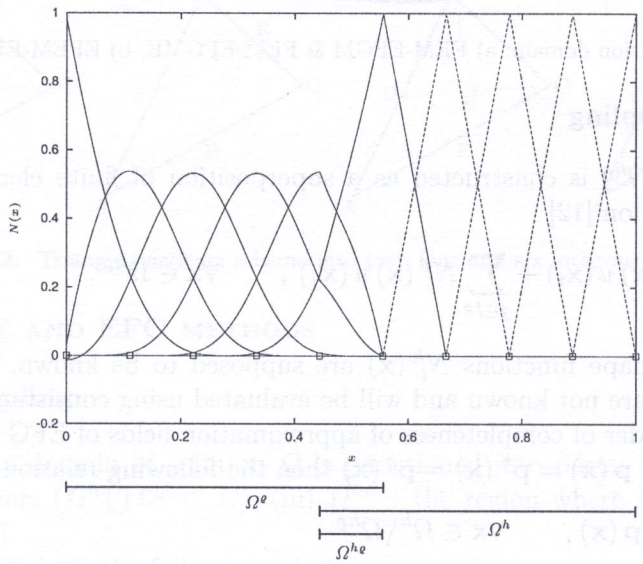

Fig. 4. Shape functions in FEM-EFGM method in 1D case

3.3. FEM-EFGME coupling

In the method, the approximation (24) is still valid, but now $\mathbf{p}^{\varrho} \neq \mathbf{p}^h$ and $\mathbf{p}^{\varrho}$ is enriched by additional base functions. In consequence, the following relations are true

$$\begin{aligned} &\sum_{i\in I^{\varrho}} \mathbf{p}^{\varrho}(\mathbf{x}_i)\,N_i^{\varrho}(\mathbf{x}) = \mathbf{p}^{\varrho}(\mathbf{x}) \quad \forall \mathbf{x}\in\Omega^{\varrho}\backslash\Omega^{h\varrho} \\ &\quad \Rightarrow \\ &\sum_{i\in I^{h}} \mathbf{p}^{\varrho}(\mathbf{x}_i)\,N_i^{h}(\mathbf{x}) = \mathbf{p}^{\varrho}(\mathbf{x}) \quad \forall \mathbf{x}\in\Omega^{h}\backslash\Omega^{h\varrho} \end{aligned} \tag{31}$$

and

$$\begin{aligned} &\sum_{i\in I^{h}} \mathbf{p}^{h}(\mathbf{x}_i)\,N_i^{h}(\mathbf{x}) = \mathbf{p}^{h}(\mathbf{x}) \quad \forall \mathbf{x}\in\Omega^{h}\backslash\Omega^{h\varrho} \\ &\quad \Rightarrow \\ &\sum_{i\in I^{\varrho}} \mathbf{p}^{h}(\mathbf{x}_i)\,N_i^{\varrho}(\mathbf{x}) = \mathbf{p}^{h}(\mathbf{x}) \quad \forall \mathbf{x}\in\Omega^{\varrho}\backslash\Omega^{h\varrho}\,. \end{aligned} \tag{32}$$

Shape functions $N_i^{\varrho}(\mathbf{x})$ are found in such a way as to recover the vector of base functions $\mathbf{p}^{\varrho}(\mathbf{x})$ in $\Omega^{h\varrho}$ part

$$\mathbf{p}^{\varrho}(\mathbf{x}) = \sum_{i \in I^h} \mathbf{p}^{\varrho}(\mathbf{x}_i) N_i^h(\mathbf{x}) + \sum_{j \in I^{\varrho}} \mathbf{p}^{\varrho}(\mathbf{x}_j) N_j^{\varrho}(\mathbf{x}) , \qquad \forall \mathbf{x} \in \Omega^{h\varrho} . \tag{33}$$

The following steps of calculations are analogous to the procedure described in point 3.2.
The shape functions for 1D case are shown in Fig. 5 assuming

$\mathbf{p}^{\varrho}(\mathbf{x}) = \{1x \sin x \sin 2x\}$ and $\mathbf{p}^h(\mathbf{x}) = \{1x\}$.

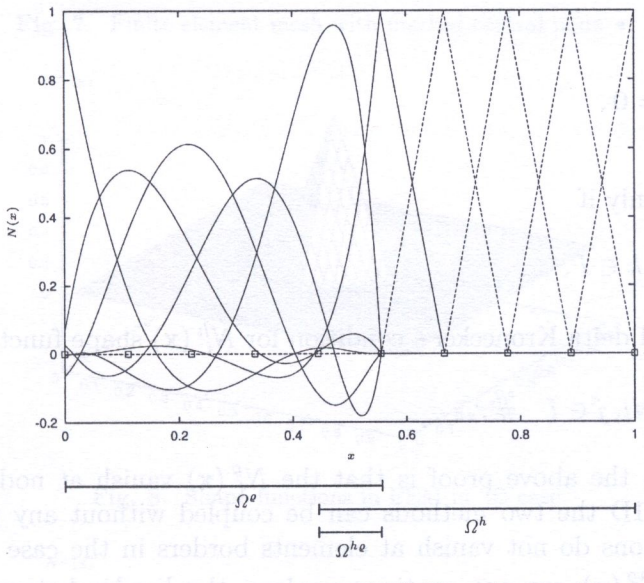

Fig. 5. Shape functions in FEM-EFGME method in 1D case

3.4. EFEM-EFGM coupling

In the method $\Omega \cong \Omega^h$ and $\Omega^{h\varrho} \subset \Omega^h$, which means that all domain Ω is covered by finite elements and in some part of Ω^h domain the approximation is enriched by shape functions of the enriched EFG method.

The procedure of computations of $N_i^{\varrho}(\mathbf{x})$ shape functions is the same as in FEM-EFGM coupling with the difference that now $N_i^h(\mathbf{x})$ shape functions are complete in $\Omega^{h\varrho}$ part.

In results of calculations the following matrix of shape function in $\Omega^{h\varrho}$ part is get

It can be proved that shape functions

$$\mathbf{N}^{h\varrho}(\mathbf{x}) = \mathbf{N}^h(\mathbf{x}) + \mathbf{N}^{\varrho}(\mathbf{x}) , \qquad \forall \mathbf{x} \in \Omega^{h\varrho} \tag{34}$$

of FEM and EFGM coupling are interpolation functions. **Proof.** The conditions of completeness for $N_i^{h\varrho}(\mathbf{x})$ have the form

$$\sum_{i \in I} \mathbf{p}^{\varrho}(\mathbf{x}_i) N_i^{h\varrho}(\mathbf{x}) = \mathbf{p}^{\varrho}(\mathbf{x}) , \qquad \forall \mathbf{x} \in \Omega^{h\varrho} , \tag{35}$$

□

or, after substitution of Eq. (34)

$$\sum_{i \in I} \mathbf{p}^{\varrho}(\mathbf{x}_i) N_i^h(\mathbf{x}) + \sum_{i \in I'} \mathbf{p}^{\varrho}(\mathbf{x}_i) N_i^{\varrho}(\mathbf{x}) = \mathbf{p}^{\varrho}(\mathbf{x}) , \qquad \forall \mathbf{x} \in \Omega^{h\varrho} . \tag{36}$$

Equation (36) is valid for every point in $\Omega^{h\varrho}$, in particular for node k

$$\sum_{i\in I} \mathbf{p}^{\varrho}(\mathbf{x}_i)\, N_i^h(\mathbf{x}_k) + \sum_{i\in I} \mathbf{p}^{\varrho}(\mathbf{x}_i)\, N_i^{\varrho}(\mathbf{x}_k) = \mathbf{p}^{\varrho}(\mathbf{x}_k)\,, \qquad \forall \mathbf{x}_k \in \Omega^{h\varrho}\,. \tag{37}$$

Shape functions $N_i^h(\mathbf{x})$ fulfil the delta Kronecker's condition and in effect Eq. (37) takes the form

$$\mathbf{p}^{\varrho}(\mathbf{x}_k) + \sum_{i\in I} \mathbf{p}^{\varrho}(\mathbf{x}_i)\, N_i^{\varrho}(\mathbf{x}_k) = \mathbf{p}^{\varrho}(\mathbf{x}_k)\,, \qquad \forall \mathbf{x}_k \in \Omega\,. \tag{38}$$

or after simplification

$$\sum_{i\in I} \mathbf{p}^{\varrho}(\mathbf{x}_i)\, N_i^{\varrho}(\mathbf{x}_k) = \mathbf{0}\,. \tag{39}$$

Equation (39) is valid only if

$$N_i^{\varrho}(\mathbf{x}_k) = 0, \qquad \forall i,k \in I\,. \tag{40}$$

On the base of (40) and delta Kronecker's condition for $N_i^h(\mathbf{x})$ shape function it can be written

$$N_i^{h\varrho}(\mathbf{x}_j) = \delta_{ij}\,, \qquad \forall i,j \in I \quad \#\,. \tag{41}$$

The conclusion from the above proof is that the $N_i^{\varrho}(\mathbf{x})$ vanish at nodes where an FE shape function is defined. In 1D the two methods can be coupled without any problem, but in 2D or 3D $N_i^{\varrho}(\mathbf{x})$ shape functions do not vanish at elements borders in the case when $\mathbf{p}^{\varrho}(\mathbf{x}) \neq \mathbf{p}^h(\mathbf{x})$. In consequence the $N_i^{h\varrho}(\mathbf{x})$ are not continuous along the border between $\Omega^h \setminus \Omega^{h\varrho}$ and $\Omega^{h\varrho}$ regions. The discontinuities in most cases are quite small, and when discretisation is denser the discontinuities are smaller and vanish at limit.

Assuming the same vectors of base functions $\mathbf{p}^{\varrho}(\mathbf{x})$ and $\mathbf{p}^h(\mathbf{x})$ as in the previous example the shape functions have been calculated and are shown in Fig. 6. Examples of shape functions in 2D for methods: FEM, EFGM and EFEM-EFGM are shown in Figs. 8, 9 and 10. These functions have been calculated for the central node shown in Fig. 7 assuming

$$\mathbf{p}^h(\mathbf{x}) = \{1 \;\; x \;\; y\} \text{ and } \mathbf{p}^{\varrho}(\mathbf{x}) = \{1 \;\; x \;\; y \sin(x)\cdot\sin(y) \;\; \sin(x)\cdot\cos(y) \;\; \cos(x\cdot y)\}.$$

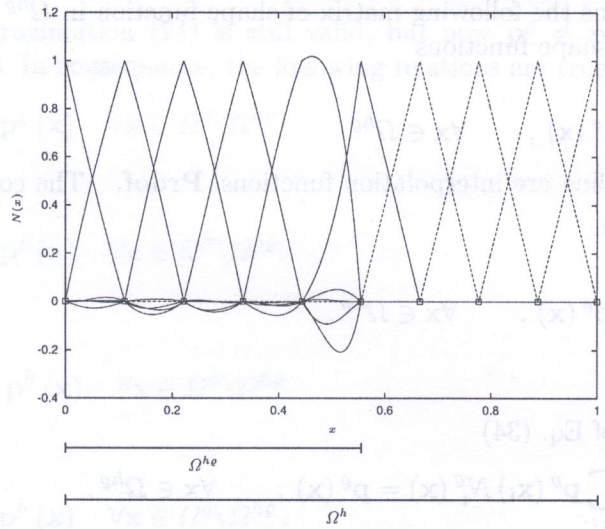

Fig. 6. Shape functions in FEM-EFGME method in 1D case

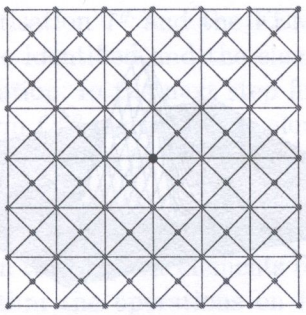

Fig. 7. Finite element mesh with marked central node •.

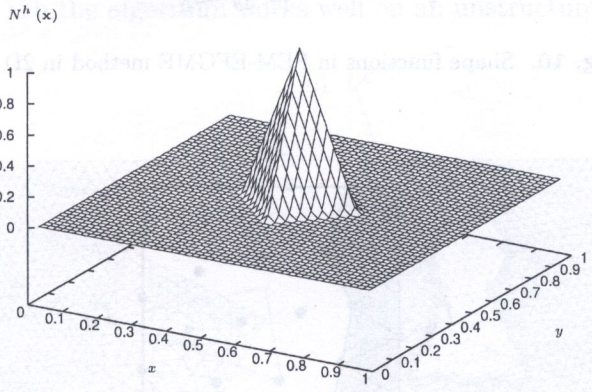

Fig. 8. Shape functions in FEM in 2D case

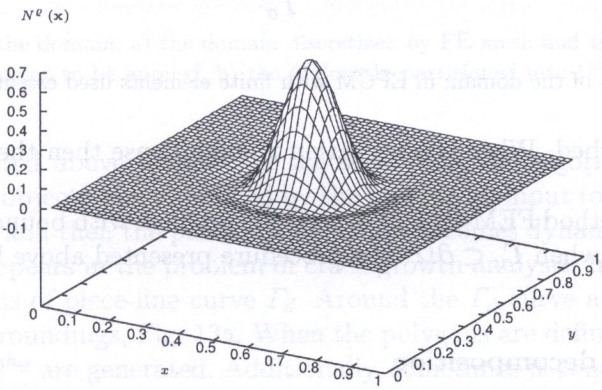

Fig. 9. Shape functions EFGM in 2D case

3.5. Essential boundary conditions

One of the main problems in EFGM is applying the essential boundary conditions and till now numerous methods to apply the boundary conditions have been developed [3, 4, 7, 15, 23]. In the paper the coupling method is used to apply the boundary conditions to EFGM.

Let us assume that $\Omega^\varrho = \Omega$. The boundary Γ is divided into Γ_σ and Γ_u where the natural and essential boundary conditions are defined respectively. Along the Γ_u the finite elements are constructed and they create the $\Omega^{h\varrho}$ area, Fig. 11. In the elements the FE shape functions are built for nodes that belong to the boundary. Since along the Γ_u shape functions satisfy the Kronecker's conditions it means that the essential boundary conditions can be applied in the same way as in FEM. It should be noted that in the case when the base functions in vector $\mathbf{p}^\varrho(\mathbf{x})$ are the same as in vector $\mathbf{p}^h(\mathbf{x})$ then the boundary conditions are satisfied exactly. In the case when the vector of base functions $\mathbf{p}^\varrho(\mathbf{x})$ is richer than $\mathbf{p}^h(\mathbf{x})$ then in 2D or 3D cases the essential boundary conditions

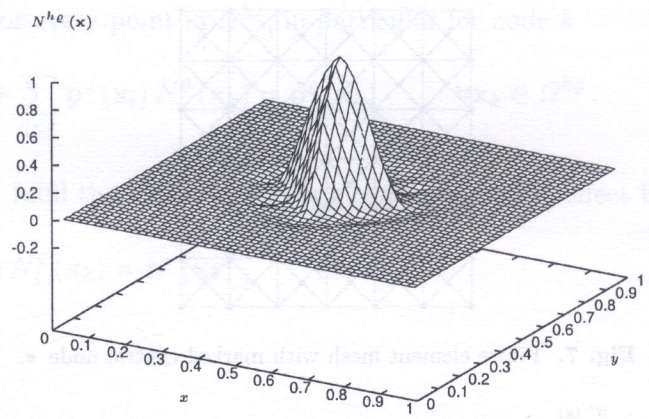

Fig. 10. Shape functions in FEM-EFGME method in 2D case

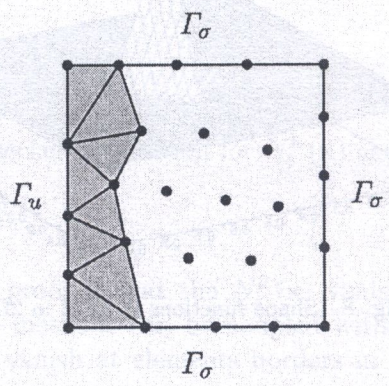

Fig. 11. Discretisation of the domain in EFGM with finite elements used essential boundary conditions

between nodes are disturbed. When discretisation is more dense then the disturbances are smaller and vanish at limit.

When the coupling method FEM-EFGM is used the problem with boundary conditions is omitted if $\Gamma_u \subset \partial\Omega^h$. In the case when $\Gamma_u \subset \partial\Omega^q$ the procedure presented above has to be applied.

3.6. Dynamic domain decomposition

As mentioned earlier, the main aim of couplin of the FEM with EFGM is to apply their advantages and hide their drawbacks at the same time. It is more reasonable to couple the methods by using the EFGM only to very specific, relatively small places. The special places can be, for example, the regions of error concentration or the regions where the character of the solution is known a priori. Therefore an algorithm is needed to partition the domain of solution Ω into Ω^h, Ω^q and Ω^{hq}. The algorithm should be simple to use and should include the possibility of dynamic change of the partition (e.g. the region around the growing crack etc.), [13].

The main assumption in the algorithm is that the FEM is the basic method which is used in analysis. At the beginning Ω is discretized with finite elements. Then information is entered to the finite element mesh about the places where EFGM should be used. The information is in the form of simple geometrical objects like polygons, circles or ellipses. The geometrical objects can be placed in an arbitrary place in the mesh, in any shape and in any relation to each other. The objects can overlap or they can go outside Ω, Fig. 12a.

In the next step of the algorithm all nodes that are inside the geometrical objects have to be identified. The nodes become nodes of element free approximation. In consequence all nodes are

grouped into nodes of EFGM discretisation I^{ϱ} and the FEM nodes I^{h}. Next, all finite elements that are defined on nodes $i_k \in I^{\varrho}$ are identified and the elements are marked with index e^{ϱ}. The e^{ϱ} elements are erased from discretisation. In the next step finite elements $e^{h\varrho}$ that are defined on nodes $i_i \in I^{\varrho} \cap I^{h}$ are marked and form $\Omega^{h\varrho}$ region. In the elements incomplete shape functions are defined. The incompleteness refers to the nodes in the elements that $i_k \in I^{\varrho}$. The final discretisation is shown in Fig. 12b.

It should be emphasized that the e^{ϱ} elements are removed only from the approximation field but they are not removed from memory. In this way the elements become simultaneously the integration cells in EFGM. In the above algorithm the operations on floating numbers appear only at the beginning of the algorithm where the nodes that are inside geometrical objects have to be found. The rest of operations have the logical character since they use connectivity table of finite elements. As shown in Fig. 12a and 12b the algorithm works well on an unstructured irregular mesh.

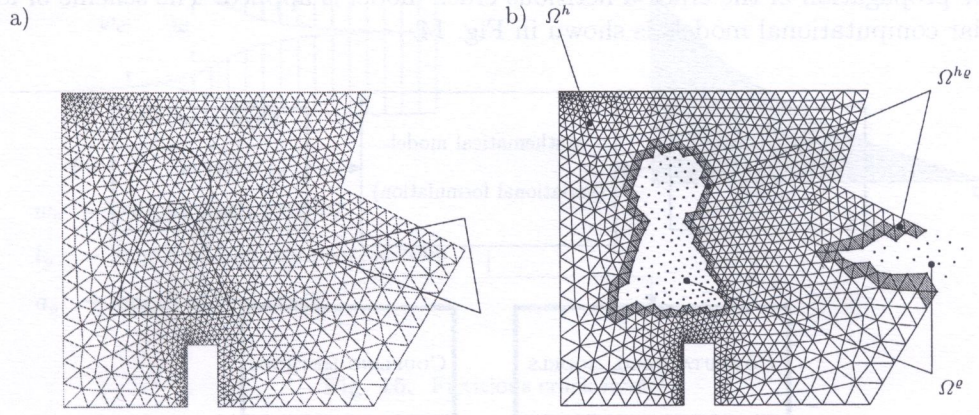

Fig. 12. Partition of the domain: a) the domain discretized by FE mesh and the marked places where EFGM is assumed to be applied, b) the Ω domain partitioned into Ω^{h}, Ω^{ϱ} and $\Omega^{h\varrho}$

The algorithm presented above is static in the sense that the algorithm works after defining geometrical objects. The objects can be defined by the user, as an input to the program, or they can be defined automatically and then the partition algorithm becomes dynamic. The need for dynamic domain decomposition appears in the problem of crack growth analysis. In such problems the crack is approximated by means of piece-line curve Γ_d. Around the Γ_d curve a polygon is automatically generated as its close surroundings, Fig. 13a. When the polygons are defined the above procedure is performed and Ω^{ϱ} and $\Omega^{h\varrho}$ are generated. Additionally, sometimes it is necessary to generate some special pattern of nodes inside Ω^{ϱ}. For instance, in the crack analysis the nodes are generated along both sides of Γ_d and around the crack tip, Fig. 13b.

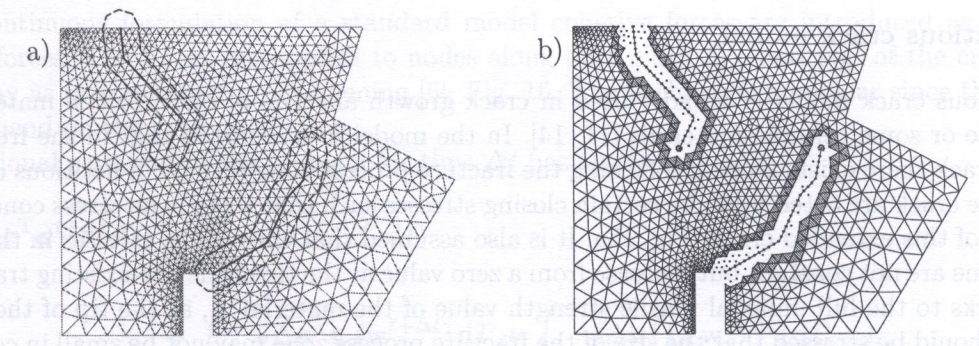

Fig. 13. Partition of the domain with cracks: a) the domain discretized by FE mesh and the marked places around lines where EFGM is assumed to be applied, b) the partitioned domain with cracks

When EFEM-EFGM method is used then the domain is partitioned into Ω^h and $\Omega^{h\varrho}$ subdomains. In such a case, in the above algorithm it is enough to mark e^{ϱ} elements as $e^{h\varrho}$. It means that no elements are removed from discretisation and there is no need to construct incomplete FEM shape functions in finite elements $e^{h\varrho}$.

4. Computational models of crack growth analysis

4.1. Computational models

In this section computational models for crack growth analysis in quasi-brittle materials in plane stress state are formed. The computational models are obtained by linking particular coupling methods with the variational formulation of the problem and with a model of crack propagation. To describe propagation of the crack a fictitious crack model is applied. The scheme of formulation of particular computational models is shown in Fig. 14.

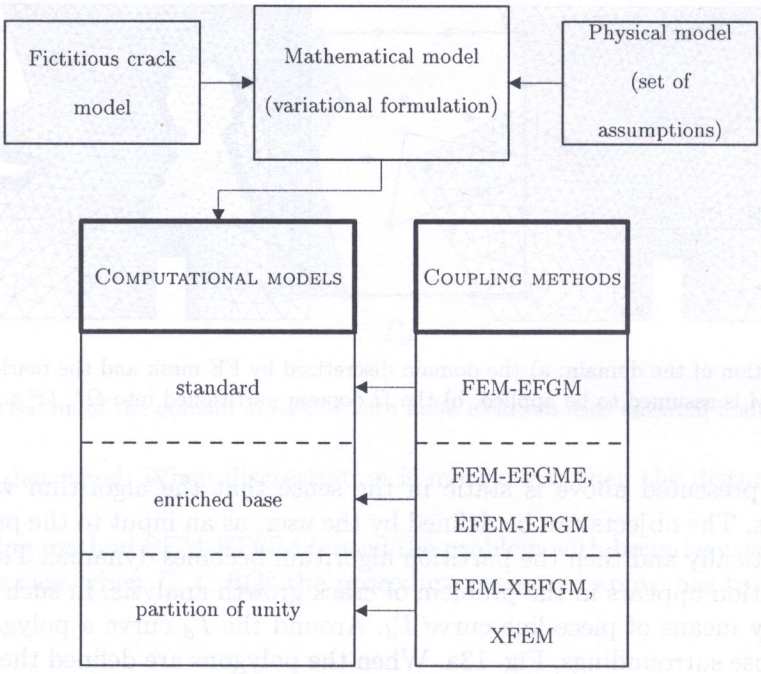

Fig. 14. Computational models of crack growth analysis

4.2. Fictitious crack model

The fictitious crack model is broadly used in crack growth analysis of quasi-brittle materials such as concrete or some ceramic materials [11, 14]. In the model it is assumed that in the front of pre-existing crack there exists tension softening the fracture process zone through a fictitious crack. The faces of the crack are acted upon be certain closing stresses such that there is no stress concentration at the tip of this extended crack, Fig. 15a. It is also assumed that the closing stresses in the fracture process zone are not constant but increase from a zero value at the tip of the pre-existing traction-free macrocracks to the full uniaxial tensile strength value of the material f_t, at the tip of the fictitious crack. It should be stressed that the size of the fracture process zone may not be small in comparison with the length of the pre-existing macrocracks and in result knowledge of the distribution of closing stress $\sigma(w)$ along the fracture process zone is essential.

The closing stresses $\sigma(w)$ are linked with the fracture energy G_F with the help of relation

$$G_F = \int_{f_t}^{0} w(\sigma)\,\mathrm{d}\sigma = \int_{0}^{w_c} \sigma(w)\,\mathrm{d}w\,, \tag{42}$$

where w_c is the critical tip opening displacement of the pre-existing macrocrack.

The $\sigma(w)$ function should be monotonically decreasing from f_t to zero and can be expressed with the help of at least two material parameters f_t and G_F, Fig. 15b.

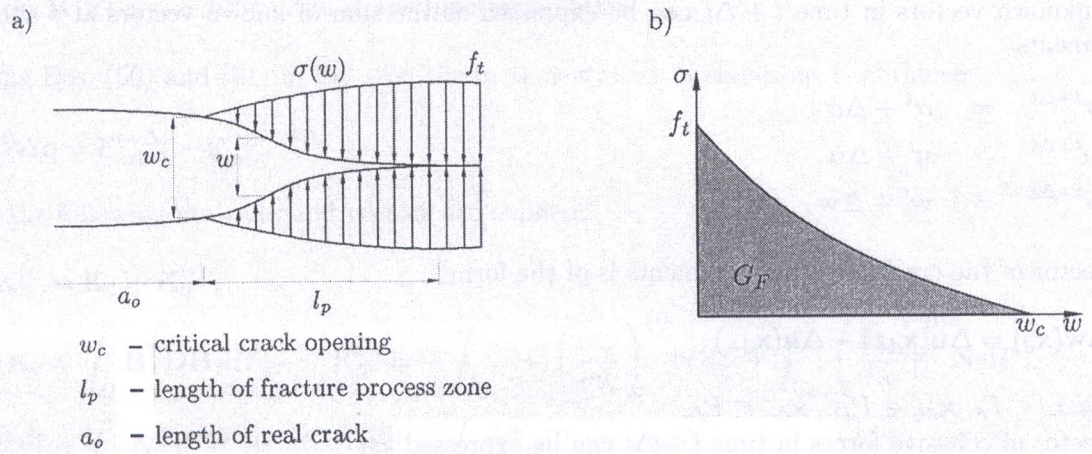

Fig. 15. Fictitious crack model

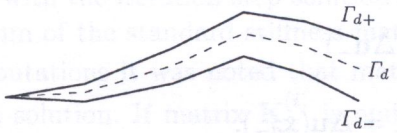

Fig. 16. Two sides Γ_{d+} i Γ_{d-} of crack Γ_d

4.3. Standard model

4.3.1. Continuous formulation

In the continuous formulation of a standard model cohesive forces are introduced as additional external forces. The forces are applied to nodes along both sides Γ_{d+} and Γ_{d-} of the crack line in such a way as to counteract crack opening [6], Fig. 16. The problem is nonlinear since the cohesive forces depend on the current solution.

Variational equation of the problem for time Δt has the form

$$\int_{\Omega} \delta\Delta\boldsymbol{\varepsilon}^{\mathrm{T}}\boldsymbol{\sigma}^{t+\Delta t}\,\mathrm{d}\Omega - \int_{\Gamma_\sigma} \delta\Delta\mathbf{u}^{\mathrm{T}}\bar{\mathbf{t}}^{t+\Delta t}\,\mathrm{d}\Gamma + \int_{\Gamma_{d-}} \delta\Delta\mathbf{u}^{\mathrm{T}}\mathbf{t}_c(\mathbf{w}^{t+\Delta t})\,\mathrm{d}\Gamma + \int_{\Gamma_{d+}} \delta\Delta\mathbf{u}^{\mathrm{T}}\mathbf{t}_c(\mathbf{w}^{t+\Delta t})\,\mathrm{d}\Gamma = 0\,, \tag{43}$$

where the body forces are omitted and

$\boldsymbol{\sigma} = \begin{pmatrix} \sigma_x & \sigma_y & \tau_{xy} \end{pmatrix}^{\mathrm{T}}$ – stress vector,
$\boldsymbol{\epsilon} = \begin{pmatrix} \varepsilon_x & \varepsilon_y & \varepsilon_{xy} \end{pmatrix}^{\mathrm{T}}$ – strain vector,
$\mathbf{u} = \begin{pmatrix} u_x & u_y \end{pmatrix}^{\mathrm{T}}$ – displacement vector,
$\bar{\mathbf{t}} = \begin{pmatrix} \bar{t}_x & \bar{t}_y \end{pmatrix}^{\mathrm{T}}$ – prescribed traction forces vector applied on Γ_σ boundary,
$\mathbf{w} = \begin{pmatrix} w_x & w_y \end{pmatrix}^{\mathrm{T}}$ – crack opening vector,
$\mathbf{t}_c = \begin{pmatrix} t_{cx} & t_{cy} \end{pmatrix}^{\mathrm{T}}$ – cohesive forces vector,
$\bar{\mathbf{u}} = \begin{pmatrix} \bar{u}_x & \bar{u}_y \end{pmatrix}^{\mathrm{T}}$ – prescribed displacement vector applied on Γ_u boundary.

Unknown vectors in time $t + \Delta t$ can be expressed as the sum of known vectors at t and their increments

$$\begin{aligned} \boldsymbol{\sigma}^{t+\Delta t} &= \boldsymbol{\sigma}^t + \Delta\boldsymbol{\sigma}\,, \\ \mathbf{u}^{t+\Delta t} &= \mathbf{u}^t + \Delta\mathbf{u}\,, \\ \mathbf{w}^{t+\Delta t} &= \mathbf{w}^t + \Delta\mathbf{w}\,. \end{aligned} \tag{44}$$

Vector of the crack opening increments is of the form

$$\Delta\mathbf{w}(\mathbf{x}_d) = \Delta\mathbf{u}(\mathbf{x}_{d+}) - \Delta\mathbf{u}(\mathbf{x}_{d-})\,, \tag{45}$$

where $\mathbf{x}_d \in \Gamma_d$, $\mathbf{x}_{d+} \in \Gamma_{d+}$, $\mathbf{x}_{d-} \in \Gamma_{d-}$.

Vector of cohesive forces in time $t + \Delta t$ can be expressed as

$$\mathbf{t}_c(\mathbf{w}^{t+\Delta t}) = \mathbf{t}_c(\mathbf{w}^t + \Delta\mathbf{w}) = \mathbf{t}_c(\mathbf{w}^t) + \Delta\mathbf{t}_c\,, \tag{46}$$

where vector of increments $\Delta\mathbf{t}_c$ is calculated from the expression

$$\Delta\mathbf{t}_c \approx \frac{\partial\mathbf{t}_c}{\partial\mathbf{w}}\Delta\mathbf{w} = \frac{\partial\mathbf{t}_c}{\partial\mathbf{w}}(\Delta\mathbf{u}_+ - \Delta\mathbf{u}_-)\,, \tag{47}$$

where $\Delta\mathbf{u}_+ = \Delta\mathbf{u}(\mathbf{x}_{d+})$ and $\Delta\mathbf{u}_- = \Delta\mathbf{u}(\mathbf{x}_{d-})$.

It is assumed that the elastic continuum obeys the Hook's law

$$\Delta\boldsymbol{\sigma} = \mathbf{D}\Delta\boldsymbol{\varepsilon}\,, \tag{48}$$

where $\mathbf{D}$ is the material stiffness matrix.

Substituting Eqs. (45–48) into (43) the following incremental variational equation is obtained

$$\begin{aligned} &\int_\Omega \delta\Delta\boldsymbol{\varepsilon}^T\mathbf{D}\Delta\boldsymbol{\varepsilon}\,\mathrm{d}\Omega + \int_{\Gamma_u} \delta\Delta\boldsymbol{\lambda}^T\Delta\mathbf{u}\,\mathrm{d}\Gamma + \int_{\Gamma_u} \delta\Delta\mathbf{u}^T\Delta\boldsymbol{\lambda}\,\mathrm{d}\Gamma \\ &\quad - \int_{\Gamma_{d+}} \delta\Delta\mathbf{u}^T\frac{\partial\mathbf{t}_c}{\partial\mathbf{w}}\Delta\mathbf{u}\,\mathrm{d}\Gamma + \int_{\Gamma_{d-}} \delta\Delta\mathbf{u}^T\frac{\partial\mathbf{t}_c}{\partial\mathbf{w}}\Delta\mathbf{u}\,\mathrm{d}\Gamma \\ &\quad = \int_{\Gamma_\sigma} \delta\Delta\mathbf{u}^T\bar{\mathbf{t}}^{t+\Delta t}\,\mathrm{d}\Gamma - \int_{\Gamma_{d-}} \delta\Delta\mathbf{u}^T\mathbf{t}_c(\mathbf{w}^t)\,\mathrm{d}\Gamma - \int_{\Gamma_{d+}} \delta\Delta\mathbf{u}^T\mathbf{t}_c(\mathbf{w}^t)\,\mathrm{d}\Gamma \\ &\quad - \int_\Omega \delta\Delta\boldsymbol{\varepsilon}^T\boldsymbol{\sigma}^t\,\mathrm{d}\Omega\,. \end{aligned} \tag{49}$$

4.3.2. Discrete formulation

In order to obtain the discrete form of Eq. (49) the following approximations are assumed.

1. *Approximation of the displacement increments vector*

$$\Delta\mathbf{u}(\mathbf{x}) = \mathbf{N}(\mathbf{x})\,\Delta\mathbf{q}, \tag{50}$$

where $\Delta\mathbf{q}$ is the vector of degrees of freedom increments.

2. *Approximation of the strain increments vector*

$$\Delta\boldsymbol{\varepsilon}(\mathbf{x}) = \mathbf{L}\mathbf{N}(\mathbf{x})\,\Delta\mathbf{q} = \mathbf{B}(\mathbf{x})\,\Delta\mathbf{q}, \tag{51}$$

where $\mathbf{B}(\mathbf{x})$ is the differential shape functions matrix.

Using Eqs. (50) and (51) in Eq. (49) the incremental set of equations is obtained

$$\mathbf{K}^{(i)}\Delta\mathbf{q} = \mathbf{F}_{\text{ext}}^{t+\Delta t} - \mathbf{F}_{\text{int}}^{(i)}, \tag{52}$$

where the following matrices and vectors are defined:

$$\begin{aligned}
&\mathbf{K}^{(i)} = \mathbf{K}_1 + \mathbf{K}_2^{(i)},\\
&\mathbf{K}_1 = \int_{\Omega}\mathbf{B}^{\mathrm{T}}\mathbf{D}\mathbf{B}\,\mathrm{d}\Omega, \qquad \mathbf{K}_2^{(i)} = -\int_{\Gamma_{d+}}\mathbf{N}^{\mathrm{T}}\left(\frac{\partial\mathbf{t}_c}{\partial\mathbf{w}}\right)^{(i)}\mathbf{N}\,\mathrm{d}\Gamma + \int_{\Gamma_{d-}}\left(\frac{\partial\mathbf{t}_c}{\partial\mathbf{w}}\right)^{(i)}\mathbf{N}\,\mathrm{d}\Gamma,\\
&\mathbf{F}_{\text{ext}}^{t+\Delta t} = \int_{\Gamma_\sigma}\mathbf{N}^{\mathrm{T}}\bar{\mathbf{t}}^{t+\Delta t}\,\mathrm{d}\Gamma, \qquad \mathbf{F}_{\text{int}}^{(i)} = \int_{\Omega}\mathbf{B}^{\mathrm{T}}\boldsymbol{\sigma}^{(i)}\,\mathrm{d}\Omega + \mathbf{F}_c^{(i)}\\
&\mathbf{F}_c^{(i)} = \int_{\Gamma_{d+}}\mathbf{N}^{\mathrm{T}}\mathbf{t}_c\big(\mathbf{w}^{(i)}\big)\,\mathrm{d}\Gamma + \int_{\Gamma_{d-}}\mathbf{N}^{\mathrm{T}}\mathbf{t}_c\big(\mathbf{w}^{(i)}\big)\,\mathrm{d}\Gamma,
\end{aligned} \tag{53}$$

and where index (i) is connected with the iteration step solution of the above equations.

Matrix $\mathbf{K}^{(i)}$ is the algebraic sum of the standard stiffness matrix $\mathbf{K}_1$ and the cohesive stiffness matrix $\mathbf{K}_2^{(i)}$. In several test computations it was noted that matrix $\mathbf{K}_2^{(i)}$ caused some oscillations in the iteration procedure of the solution. If matrix $\mathbf{K}_2^{(i)}$ is omitted, the monotonic convergence is observed even for a small number of iteration steps. Additionally, omitting matrix $\mathbf{K}_2^{(i)}$ can significantly simplify the calculations. Therefore in the examples the matrix $\mathbf{K}_2^{(i)}$ was neglected. The iteration procedure was always converged because the vector of residuum was properly calculated.

The region Ω^{ϱ} in the standard model was built as the close neighborhood of the crack line. During crack growing the region Ω^{ϱ} was updated dynamically, explained in point 3.6. The crack Γ_d was modelled with the help of the diffraction method [5].

4.4. Enriched base model

4.4.1. Continuous formulation

The variational equation of the problem for time $t + \Delta t$ now takes the form

$$\int_{\Omega}\delta\Delta\boldsymbol{\varepsilon}^{T}\boldsymbol{\sigma}^{t+\Delta t}\,\mathrm{d}\Omega - \int_{\Gamma_\sigma}\delta\Delta\mathbf{u}^{T}\bar{\mathbf{t}}^{t+\Delta t}\,\mathrm{d}\Gamma = 0. \tag{54}$$

The displacement vector $\mathbf{u}(\mathbf{x})$ is supposed to be discontinuous along curve Γ_d, that is why the vector of strain increments is expressed

$$\Delta\boldsymbol{\varepsilon}(\mathbf{x}) = \mathbf{L}\Delta\mathbf{u}(\mathbf{x}) + \delta_{\Gamma_d}\mathbf{n}\Delta[\![\mathbf{u}]\!] = \Delta\hat{\boldsymbol{\varepsilon}} + \delta_{\Gamma_d}\mathbf{n}\Delta[\![\mathbf{u}]\!], \tag{55}$$

where $[\![\bullet]\!]$ is the function jump operator, δ_{Γ_d} is the Dirac delta along Γ_d and

$$\mathbf{n} = \begin{bmatrix} n_x & 0 \\ 0 & n_y \\ n_y & n_x \end{bmatrix}, \tag{56}$$

where n_x, n_y are coordinates of the normalized vector normal to Γ_d.

The opening crack vector $\mathbf{w}(\mathbf{x})$ and its increment are of the form

$$\mathbf{w}(\mathbf{x}) := [\![\mathbf{u}]\!](\mathbf{x}), \qquad \Delta\mathbf{w}(\mathbf{x}) := \Delta[\![\mathbf{u}]\!](\mathbf{x}). \tag{57}$$

Substituting Eq. (55) to Eq. (54) and taking advantage of the Dirac delta property

$$\int_{\Omega} \delta\Big(\delta_{\Gamma_d}\Delta[\![\mathbf{u}]\!]\Big)^{\mathrm{T}}\mathbf{n}^{\mathrm{T}}\boldsymbol{\sigma}^{t+\Delta t}\,\mathrm{d}\Omega = \int_{\Gamma_d}\delta\Delta[\![\mathbf{u}]\!]^{\mathrm{T}}\mathbf{t}_c\Big([\![\mathbf{u}]\!]^{t+\Delta t}\Big)\,\mathrm{d}\Gamma \tag{58}$$

results in

$$\int_{\Omega}\delta\Delta\hat{\boldsymbol{\varepsilon}}^{\mathrm{T}}\boldsymbol{\sigma}^{t+\Delta t}\,\mathrm{d}\Omega + \int_{\Gamma_d}\delta\Delta[\![\mathbf{u}_2]\!]^{\mathrm{T}}\mathbf{t}_c\Big([\![\mathbf{u}]\!]^{t+\Delta t}\Big)\,\mathrm{d}\Gamma = \int_{\Gamma_\sigma}\delta\Delta\mathbf{u}^{\mathrm{T}}\overline{\mathbf{t}}^{t+\Delta t}\,\mathrm{d}\Gamma, \tag{59}$$

where $\mathbf{t}_c\Big([\![\mathbf{u}]\!]^{t+\Delta t}\Big)$ is the cohesive forces vector distributed along the crack line Γ_d. It can be noted that the vector of cohesive forces appeared again in the variational equation but now it is described directly on Γ_d.

Unknown vectors in time $t+\Delta t$ are obtained from Eq. (44) and from formula

$$\begin{aligned} &[\![\mathbf{u}]\!]^{t+\Delta t} = [\![\mathbf{u}]\!]^{t} + \Delta[\![\mathbf{u}]\!], \\ &\mathbf{t}_c\Big([\![\mathbf{u}]\!]^{t+\Delta t}\Big) = \mathbf{t}_c\Big([\![\mathbf{u}]\!] + \Delta[\![\mathbf{u}_2]\!]\Big) = \mathbf{t}_c\Big([\![\mathbf{u}]\!]^{t}\Big) + \Delta\mathbf{t}_c\Big([\![\mathbf{u}]\!]^{t}\Big), \end{aligned} \tag{60}$$

where

$$\Delta\mathbf{t}_c\Big([\![\mathbf{u}]\!]^{t}\Big) \approx \frac{\partial\mathbf{t}_c}{\partial[\![\mathbf{u}]\!]}\Big([\![\mathbf{u}]\!]^{t}\Big)\Delta[\![\mathbf{u}]\!].$$

The incremental constitutive equation has the form

$$\Delta\boldsymbol{\sigma} = \mathbf{D}\Delta\hat{\boldsymbol{\varepsilon}}. \tag{61}$$

Finally, substituting Eqs. (44), (60) and (61) to Eq. (59) the following incremental variational equation is obtained

$$\begin{aligned} &\int_{\Omega}\delta\Delta\hat{\boldsymbol{\varepsilon}}^{T}\mathbf{D}_T\Delta\hat{\boldsymbol{\varepsilon}}\,\mathrm{d}\Omega + \int_{\Gamma_d}\delta\Delta[\![\mathbf{u}]\!]^{T}\frac{\partial\mathbf{t}_c}{\partial[\![\mathbf{u}]\!]}\Big([\![\mathbf{u}]\!]^{t}\Big)\Delta[\![\mathbf{u}]\!]\,\mathrm{d}\Gamma \\ &\qquad = \int_{\Gamma_\sigma}\delta\Delta\mathbf{u}^{T}\overline{\mathbf{t}}^{t+\Delta t}\,\mathrm{d}\Gamma - \int_{\Omega}\delta\Delta\hat{\boldsymbol{\varepsilon}}^{T}\boldsymbol{\sigma}^{t}\,\mathrm{d}\Omega - \int_{\Gamma_d}\delta\Delta[\![\mathbf{u}]\!]^{T}\mathbf{t}_c\Big([\![\mathbf{u}]\!]^{t}\Big)\,\mathrm{d}\Gamma. \end{aligned} \tag{62}$$

4.4.2. Discrete formulation

In this computational model it is assumed that some base functions in vector $\mathbf{p}^{\varrho}(\mathbf{x})$ are discontinuous along curve Γ_d. The discretisation procedure is analogous to the procedure in point 4.3.2 with additional approximations.

1. *Approximation of the crack opening vector*

$$\Delta[\![\mathbf{u}]\!](\mathbf{x}) = [\![\mathbf{N}]\!](\mathbf{x})\,\Delta\mathbf{q}. \tag{63}$$

2. *Approximation of the strain increments vector*

$$\Delta\hat{\boldsymbol{\varepsilon}}(\mathbf{x}) = \mathbf{B}(\mathbf{x})\,\Delta\mathbf{q}. \tag{64}$$

Using Eqs. (50), (63) and (64) in Eq. (62) the set of incremental matrix equations (52) is obtained where matrices and vectors are now defined

$$\begin{aligned}
\mathbf{K}^{(i)} &= \int_{\Omega} \mathbf{B}^{\mathrm{T}}\mathbf{D}\mathbf{B}\,\mathrm{d}\Omega + \int_{\Gamma_d} [\![\mathbf{N}]\!]^T \left(\frac{\partial \mathbf{t}_c}{\partial [\![\mathbf{u}]\!]}\right)^{(i)} [\![\mathbf{N}]\!]\,\mathrm{d}\Gamma,\\
\mathbf{F}_{\mathrm{ext}}^{t+\Delta t} &= \int_{\Gamma_\sigma} \mathbf{N}^{\mathrm{T}}\bar{\mathbf{t}}^{t+\Delta t}\,\mathrm{d}\Gamma, \qquad \mathbf{F}_{\mathrm{int}}^{(i)} = \int_{\Omega} \mathbf{B}^T\boldsymbol{\sigma}^{(i)}\,\mathrm{d}\Omega + \mathbf{F}_c^{(i)},\\
\mathbf{F}_c^{(i)} &= \int_{\Gamma_d} [\![\mathbf{N}]\!]^{\mathrm{T}}\mathbf{t}_c\big(\mathbf{w}^{(i)}\big)\,\mathrm{d}\Gamma.
\end{aligned} \tag{65}$$

It can be seen that the difference between the enriched base model and standard model lies in the way in which the shape functions are calculated, in the definition of the tangent stiffness matrix $\mathbf{K}^{(i)}$ and in the definition of vector of the cohesive forces $\mathbf{F}_c^{(i)}$. In the examples the second part of matrix $\mathbf{K}^{(i)}$ was omitted with the same arguments as explained in point 4.3.2.

Matrix $[\![\mathbf{N}]\!]$ has to be evaluated in the integration points Γ_d. Assuming that $\Gamma_d \subset \Omega^{\varrho} \setminus \Omega^{h\varrho}$

$$[\![\mathbf{N}]\!](\mathbf{x}) = [\![\mathbf{N}^{\varrho}]\!](\mathbf{x}), \qquad \forall \mathbf{x} \in \Gamma_d. \tag{66}$$

In the paper matrix $[\![\mathbf{N}]\!]$ was calculated with the help of some modifications of Eqs. (10) and (11) which take the form

$$[\![\mathbf{p}]\!](\mathbf{x}) = \sum_{j=1}^{J} \mathbf{p}(\mathbf{x}_j)\,[\![N_j^{\varrho}]\!](\mathbf{x}), \qquad \forall \mathbf{x} \in \Gamma_d, \tag{67}$$

$$[\![N_j^{\varrho}]\!](\mathbf{x}) = \mathbf{p}(\mathbf{x}_j)^T\,[\![\boldsymbol{\alpha}]\!](\mathbf{x})\,w(r_j), \qquad \forall \mathbf{x} \in \Gamma_d. \tag{68}$$

Substituting Eq. (68) into Eq. (67) the following set of equations for calculation of $[\![\boldsymbol{\alpha}]\!]$ is obtained

$$\mathbf{M}(\mathbf{x})\,[\![\boldsymbol{\alpha}]\!](\mathbf{x}) = [\![\mathbf{p}]\!](\mathbf{x}), \qquad \forall \mathbf{x} \in \Gamma_d, \tag{69}$$

where

$$\mathbf{M}(\mathbf{x}) = \sum_{i=1}^{n} \mathbf{p}(\mathbf{x}_i)\,\mathbf{p}(\mathbf{x}_i)^T\,w(r_i), \qquad \forall \mathbf{x} \in \Gamma_d.$$

It should be noted that Eqs (66) to (69) are also valid when $\Gamma_d \subset \Omega^{h\varrho}$, which is the consequence of $N_i^h(\mathbf{x}) \in C^0$, so

$$[\![\mathbf{N}^h]\!](\mathbf{x}) \equiv \mathbf{0}, \qquad \forall \mathbf{x} \in \Gamma_d. \tag{70}$$

In the crack growth analysis to enrich the EFG shape functions the functions known from linear fracture mechanics are often used, Fig. 17

$$\gamma_1(\mathbf{x}) = \sqrt{r}\,\cos\left(\frac{\theta}{2}\right), \qquad \gamma_2(\mathbf{x}) = \sqrt{r}\,\sin\left(\frac{\theta}{2}\right). \tag{71}$$

In general Γ_d can be quite an arbitrary curve and an algorithm of computations of functions (71) along the curved line is needed [2, 10].

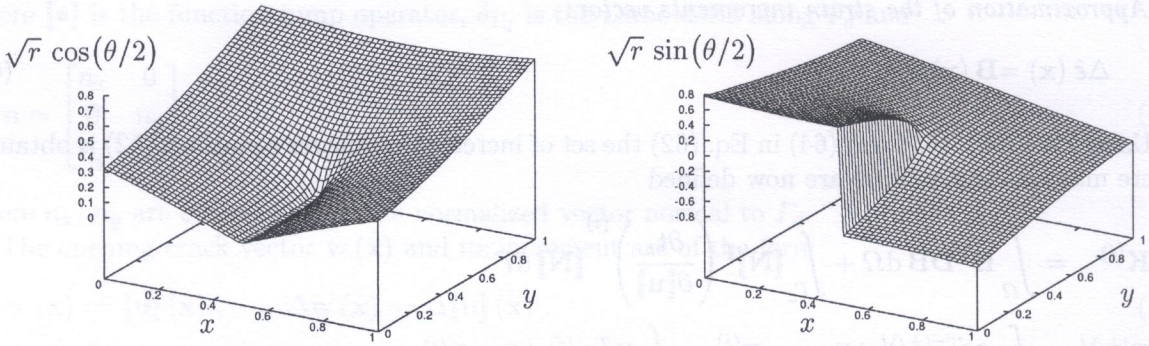

Fig. 17. Enriching functions $\gamma_1(\mathbf{x})$ i $\gamma_2(\mathbf{x})$ for straight crack line

4.5. Partition of unity model

4.5.1. Continuous formulation

In the model it is assumed that the displacement vector is a superposition of the continuous part $\mathbf{u}_1(\mathbf{x})$ and the discontinuous one $\mathbf{u}_2(\mathbf{x})$ along Γ_d

$$\mathbf{u}(\mathbf{x}) = \mathbf{u}_1(\mathbf{x}) + \mathbf{u}_2(\mathbf{x}, \Gamma_d) \,. \tag{72}$$

As the starting point the variational equation of problem (54) is assumed. The increments of the displacement vector $\Delta\mathbf{u}(\mathbf{x})$ and the strain vector $\Delta\boldsymbol{\varepsilon}(\mathbf{x})$ have the form

$$\begin{aligned} \Delta\mathbf{u}(\mathbf{x}) &= \Delta\mathbf{u}_1(\mathbf{x}) + \Delta\mathbf{u}_2(\mathbf{x}, \Gamma_d) \,, \\ \Delta\boldsymbol{\varepsilon}(\mathbf{x}) &= \mathbf{L}\Delta\mathbf{u}_1(\mathbf{x}) + \mathbf{L}\Delta\mathbf{u}_2(\mathbf{x}, \Gamma_d) + \delta_{\Gamma_d}\mathbf{n}\Delta[\![\mathbf{u}_2]\!] = \Delta\hat{\boldsymbol{\varepsilon}} + \delta_{\Gamma_d}\mathbf{n}\Delta[\![\mathbf{u}_2]\!] \,. \end{aligned} \tag{73}$$

Proceeding in an analogous way as in points 4.3.1 and 4.4.1 the following incremental variational equation is obtained

$$\begin{aligned} &\int_\Omega \delta\Delta\hat{\boldsymbol{\varepsilon}}^{\mathrm{T}}\mathbf{D}_T\Delta\hat{\boldsymbol{\varepsilon}}\,\mathrm{d}\Omega + \int_{\Gamma_d} \delta\Delta[\![\mathbf{u}_2]\!]^{\mathrm{T}} \frac{\partial \mathbf{t}_c}{\partial[\![\mathbf{u}_2]\!]}\Big([\![\mathbf{u}_2]\!]^t\Big)\Delta[\![\mathbf{u}_2]\!]\,\mathrm{d}\Gamma \\ &\quad = \int_{\Gamma_\sigma} \delta\Delta\mathbf{u}^{\mathrm{T}}\bar{\mathbf{t}}^{t+\Delta t}\,\mathrm{d}\Gamma - \int_\Omega \delta\Delta\hat{\boldsymbol{\varepsilon}}^{\mathrm{T}}\boldsymbol{\sigma}^t\,\mathrm{d}\Omega - \int_{\Gamma_d} \delta\Delta[\![\mathbf{u}_2]\!]^{\mathrm{T}}\mathbf{t}_c\Big([\![\mathbf{u}_2]\!]^t\Big)\,\mathrm{d}\Gamma \,. \end{aligned} \tag{74}$$

4.5.2. Discrete formulation

The discrete form of Eq. (74) is obtained assuming the following approximations.

1. *Approximation of the displacement increments vector*, Eq. (22)

$$\begin{aligned} \Delta\mathbf{u}(\mathbf{x}) &= \Delta\mathbf{u}_1 + \Delta\mathbf{u}_2 \\ &= \mathbf{N}(\mathbf{x})\Delta\mathbf{a} + \sum_{k=1}^{K} \gamma_k(\mathbf{x})\mathbf{N}(\mathbf{x})\mathcal{B}\Delta\mathbf{b}_k \\ &= \mathbf{N}(\mathbf{x})\Delta\mathbf{a} + \widehat{\mathbf{N}}(\mathbf{x})\Delta\mathbf{b} \,, \end{aligned} \tag{75}$$

where $\Delta\mathbf{a}$ is the vector of standard degrees of freedom, $\Delta\mathbf{b}$ contains additional degrees of freedom connected with enriching functions $\gamma_k(\mathbf{x})$.

2. *Approximation of the crack opening increments vector*

$$\Delta[\![\mathbf{u}_2]\!](\mathbf{x}) = \sum_{k=1}^{K} [\![\gamma_k]\!](\mathbf{x})\mathbf{N}(\mathbf{x})\mathcal{B}\Delta\mathbf{b}_k = \widehat{\mathbf{N}}(\mathbf{x})\Delta\mathbf{b} \,. \tag{76}$$

3. *Approximation of the strain increments vector*

$$\Delta\hat{\boldsymbol{\varepsilon}}(\mathbf{x}) = \mathbf{B}(\mathbf{x})\,\Delta\mathbf{a} + \sum_{k=1}^{K} \overline{\mathbf{B}}_k(\mathbf{x})\,\mathcal{B}\Delta\mathbf{b}_k = \mathbf{B}(\mathbf{x})\,\Delta\mathbf{a} + \widehat{\mathbf{B}}(\mathbf{x})\,\Delta\mathbf{b}, \tag{77}$$

where

$$\begin{aligned}
\mathbf{B}(\mathbf{x}) &= \mathbf{L}\mathbf{N}(\mathbf{x}), \\
\overline{\mathbf{B}}_k(\mathbf{x}) &= \mathbf{G}_k(\mathbf{x})\,\mathbf{N}(\mathbf{x}) + \gamma_k(\mathbf{x})\,\mathbf{B}(\mathbf{x}), \\
\mathbf{G}_k(\mathbf{x}) &= \begin{bmatrix} \dfrac{\partial\gamma_k(\mathbf{x})}{\partial x} & 0 \\ 0 & \dfrac{\partial\gamma_k(\mathbf{x})}{\partial y} \\ \dfrac{\partial\gamma_k(\mathbf{x})}{\partial y} & \dfrac{\partial\gamma_k(\mathbf{x})}{\partial x} \end{bmatrix}.
\end{aligned} \tag{78}$$

Using Eqs. (61) and (75) to (78) in Eq. (74) a set of the incremental matrix equation is obtained

$$\begin{bmatrix} \mathbf{K}_{11} & \mathbf{K}_{12} \\ \mathbf{K}_{21} & \mathbf{K}_{22}^{(i)} \end{bmatrix} \begin{bmatrix} \Delta\mathbf{a} \\ \Delta\mathbf{b} \end{bmatrix} = \begin{bmatrix} \mathbf{F}_{1\text{ext}}^{t+\Delta t} - \mathbf{F}_{1\text{int}}^{(i)} \\ \mathbf{F}_{2\text{ext}}^{t+\Delta t} - \mathbf{F}_{2\text{int}}^{(i)} \end{bmatrix}, \tag{79}$$

where the following matrices and vectors are defined:

$$\begin{aligned}
\mathbf{K}_{11} &= \int_{\Omega} \mathbf{B}^{\mathrm{T}}\mathbf{D}_T\mathbf{B}\,\mathrm{d}\Omega, \qquad \mathbf{K}_{12} = \int_{\Omega} \mathbf{B}^{\mathrm{T}}\mathbf{D}_T\widehat{\mathbf{B}}\,\mathrm{d}\Omega, \\
\mathbf{K}_{21} &= \mathbf{K}_{12}{}^{\mathrm{T}}, \\
\mathbf{K}_{22}^{(i)} &= \int_{\Omega} \widehat{\mathbf{B}}^{\mathrm{T}}\mathbf{D}_T\widehat{\mathbf{B}}\,\mathrm{d}\Omega + \int_{\Gamma_d} \widehat{\mathbf{N}}^{\mathrm{T}} \left(\frac{\partial \mathbf{t}_c}{\partial[\![\mathbf{u}_2]\!]}\right)^{(i)} \widehat{\mathbf{N}}\,\mathrm{d}\Gamma, \\
\mathbf{F}_{1\text{ext}}^{t+\Delta t} &= \int_{\Gamma_n} \mathbf{N}^{\mathrm{T}}\overline{\mathbf{t}}^{t+\Delta t}\,\mathrm{d}\Gamma, \qquad \mathbf{F}_{2\text{ext}}^{t+\Delta t} = \int_{\Gamma_n} \widehat{\mathbf{N}}^{\mathrm{T}}\overline{\mathbf{t}}^{t+\Delta t}\,\mathrm{d}\Gamma, \\
\mathbf{F}_{1\text{int}}^{(i)} &= \int_{\Omega} \mathbf{B}^{\mathrm{T}}\boldsymbol{\sigma}^{(i)}\,\mathrm{d}\Omega, \qquad \mathbf{F}_{2\text{int}}^{(i)} = \int_{\Omega} \widehat{\mathbf{B}}^{\mathrm{T}}\boldsymbol{\sigma}^{(i)}\,\mathrm{d}\Omega + \int_{\Gamma_d} \widehat{\mathbf{N}}^{\mathrm{T}}\mathbf{t}_c\left([\![\mathbf{u}_2]\!]^{(i)}\right)\mathrm{d}\Gamma.
\end{aligned} \tag{80}$$

The incremental set of Eqs. (79) is more complicated in comparison with Eq. (52) since additional degrees of freedom have been introduced to the approximation. In the examples, the part of the tangent stiffness matrix connected with the cohesive forces has also been neglected.

The set of equations (79) has a general form, which means that it is true for XFEM ($\Omega^{\varrho} = \emptyset$) and FEM-XEFGM ($\Omega^{\varrho} \neq \emptyset$).

4.6. Iteration method of incremental solution

The system of incremental Eqs. (52) and (79) under load control can be written in a general form, Fig. 18

$$\left.\begin{aligned}
\overline{\mathbf{K}}^{(n,i-1)}\Delta\overline{\mathbf{Q}}^{(i)} &= \overline{\mathbf{F}}_{\text{ext}}^{(n)} - \overline{\mathbf{F}}_{\text{int}}^{(i-1)} \\
\overline{\mathbf{Q}}^{(i)} &= \overline{\mathbf{Q}}^{(i-1)} + \Delta\overline{\mathbf{Q}}^{(i)}
\end{aligned}\right\}, \quad i = 1, 2, 3, \ldots \tag{81}$$

where $\overline{\mathbf{Q}}^{(i)}$ is the extended vector of degrees of freedom of the problem after the i-th iteration in step number n and $\Delta\overline{\mathbf{Q}}^{(i)}$ is the correction vector applied in the i-th iteration.

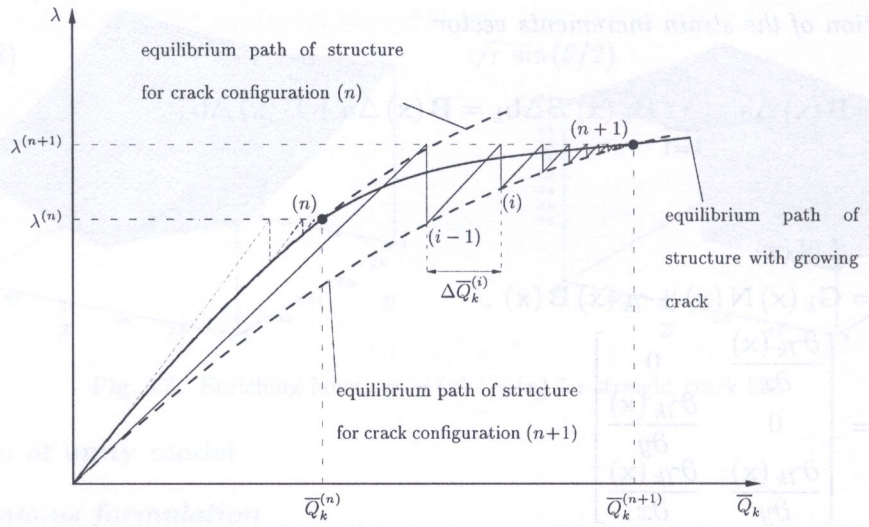

Fig. 18. Iteration method of incremental solution

It is assumed that the external load is proportional to the load parameter λ

$$\overline{\mathbf{F}}_{\text{ext}} = \lambda \overline{\mathbf{F}}^{o}_{\text{ext}}\,, \tag{82}$$

where $\overline{\mathbf{F}}^{o}_{\text{ext}}$ is a given reference load vector. In result of the Newton–Raphson iteration process at the end of step n the load level and the current crack configuration of the structure are computed.

In numerical solution the incremental Eq. (81) was coupled with the linear constraint equation of the Riks–Wempner type [17, 22], which enabled us to use different control parameters of the computation process, namely: load control, displacement control or arc-length control. The solution for each step n was realized starting from the current crack configuration and the fully unloaded structure. Such approach was applied because during crack growth the discretisation of the domain solution changes, which means that the mesh of the integration points also changes. In the authors' opinion it is a simpler approach than the recovery of the computations memory in the new mesh of integration points.

5. Examples

5.1. L–shaped domain

The problem under consideration is defined by the Laplace equation with the essential and natural boundary conditions [20]

$$\begin{aligned} -\Delta u(\mathbf{x}) &= 0, && \mathbf{x} \in \Omega\,, \\ u(\mathbf{x}) &= 0\,, && \mathbf{x} \in \Gamma_{\mathbf{e}}\,, \\ \frac{\partial u(\mathbf{x})}{\partial \mathbf{n}} &= g(\mathbf{x})\,, && \mathbf{x} \in \Gamma_{\mathbf{n}}\,, \end{aligned} \tag{83}$$

where Ω is the L–shaped domain shown in Fig. 19 and $g(x)$ is given from the exact solution

$$u(\mathbf{x}) = r^{1/3} \sin\left(\frac{\theta}{3}\right). \tag{84}$$

The solution has a singular point at origin since at this point the derivatives of the solution go to infinity. The FEM solution results in quite big errors in the vicinity or origin. In order to

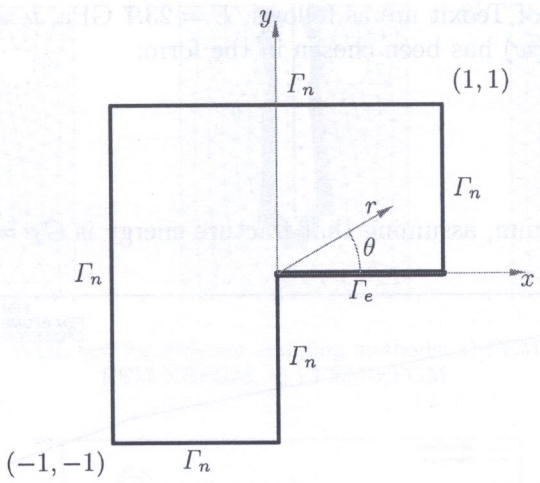

Fig. 19. L-shaped domain with (r, θ) polar coordinates with the centre at the origin

reduce the errors, the vicinity of origin has been enriched with EFGME. The analysis has been performed with FEM-EFGME and EFEM-EFGM methods. The Ω is decomposed in such a way that Ω^{ϱ} or $\Omega^{h\varrho}$ are located around the origin. In Ω^h triangular finite elements were used; it means that $\mathbf{p}^h(\mathbf{x}) = \begin{bmatrix} 1 & x & y \end{bmatrix}$. It has been assumed that the character of the solution is known *a priori* and in the example as a special function enriching $\mathbf{p}^{\varrho}(\mathbf{x})$ the exact solution is taken, so that in Ω^{ϱ} and $\Omega^{h\varrho}$ vector of EFGM base function is of the form $\mathbf{p}^{\varrho}(\mathbf{x}) = \begin{bmatrix} 1 & x & y & r^{1/3}\sin\left(\theta/3\right) \end{bmatrix}$. In such a case calculation errors in the vicinity of origin are generated only because of numerical integration.

The calculations were performed with three meshes with 166, 652, 1106 nodes, respectively. The discretisation for mesh with 1106 nodes for FEM-EFGM and EFEM-EFGM methods are shown in Fig. 20.

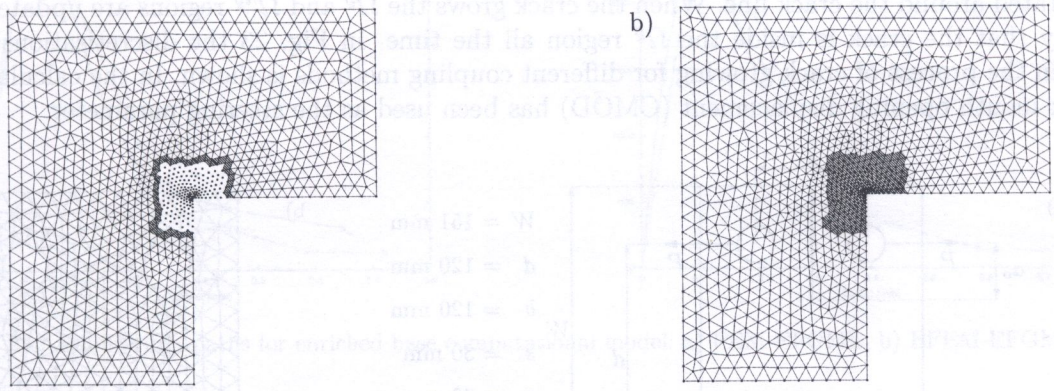

Fig. 20. L-shape domain discretisations for FEM-EFGME and EFEM-EFGM methods: a) FEM-EFGME, b) EFEM-EFGM

The errors of calculations for FEM, FEM-EFGME and EFEM-EFGM methods are shown in Fig. 21. The enriched part of domain was relatively small but, as can be seen, that resulted in large reduction in errors in comparison with FEM solution.

5.2. Wedge opening loaded test

The crack growth in wedge opening loaded test (WOL) a specimen made of ceramic material Teoxit was analyzed experimentally [21]. In Fig. 22a the geometry and load of the specimen are shown.

The material properties of Teoxit are as follows: $E = 23.7$ GPa, $\nu = 0.25$, $f_t = 5.2$ MPa. In the example the relation $\sigma = f(w)$ has been chosen in the form:

$$\sigma(w) = f_t\left(1 - \frac{w}{w_c}\right)^n, \tag{85}$$

where $n = 14$ and $w_c = 0.5\,\text{mm}$, assuming that fracture energy is $G_F = 176.6\,\text{Nm/m}^2$.

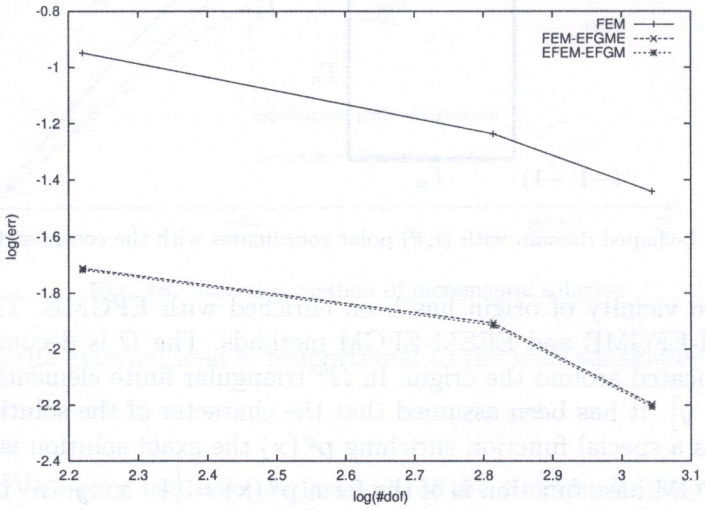

Fig. 21. Errors of FEM-EFGME and EFEM-EFGM coupling in relation to degrees of freedom #dof

The domain of solution has been initially discretized with finite elements, Fig. 22b. The mesh consists of 329 nodes and 584 finite elements. In the calculations the Ω^{ϱ} and $\Omega^{h\varrho}$ regions are generated around the crack line. When the crack grows the Ω^{ϱ} and $\Omega^{h\varrho}$ regions are updated in such a way that the crack is inside the Ω^{ϱ} region all the time. In Fig. 23 the discretisations of WOL test in the process of crack growing for different coupling methods is shown. In the calculations the crack mouth opening displacement (CMOD) has been used as the steering parameter.

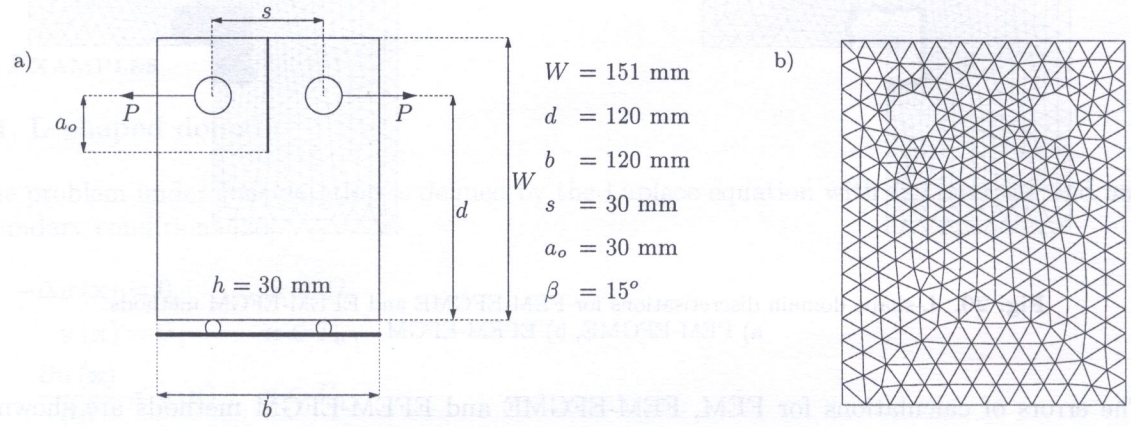

Fig. 22. The WOL test geometry and discretisation: a) The WOL test geometry, b) The WOL test discretized with finite elements

The results of calculations, in the form of equilibrium paths of the structure with a growing crack, obtained with the help of the three computational models are shown in Figs. 24, 25, 26 and compared with the experimental data. Additionally, in Fig. 26b the results of calculations using XFEM are presented. As can be seen in the pictures, the results of calculations are quite satisfactory except the analysis using the EFEM-EFGM coupling method, where great discrepancies are observed.

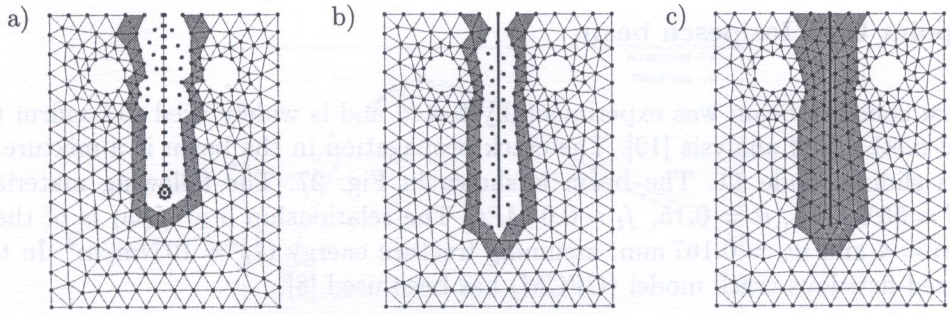

Fig. 23. Discretisation of WOL test for different coupling methods: a) FEM-EFGM, b) FEM-EFGME, FEM-XEFGM, c) EFEM-EFGM

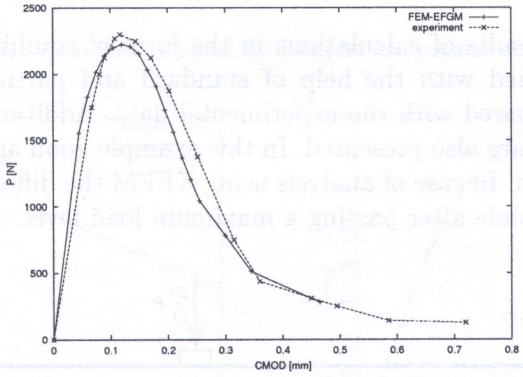

Fig. 24. Equilibrium paths for standart computational model

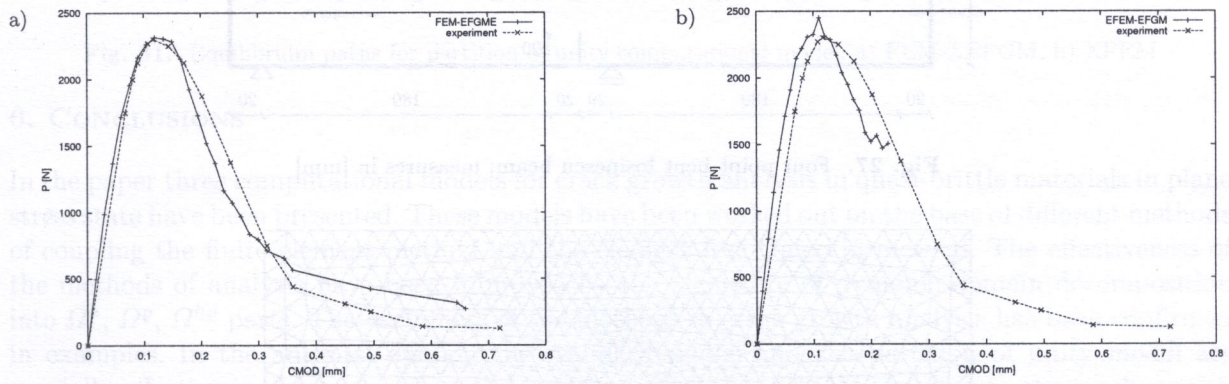

Fig. 25. Equilibrium paths for enriched base computational model: a) FEM-EFGME, b) EFEM-EFGM

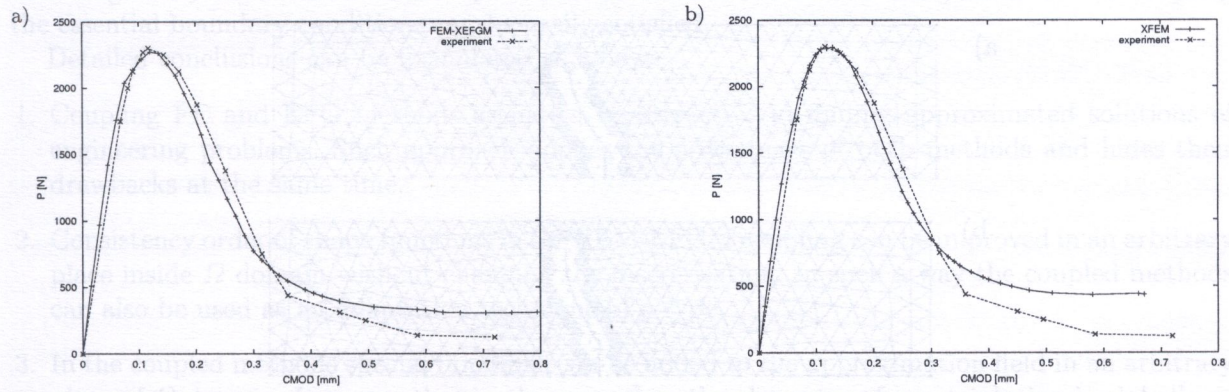

Fig. 26. Equilibrium paths for partition of unity computational model: a) FEM-EFGM-PU, b) FEM-PU

5.3. Four point bent Iosipescu beam

The Iosipescu concrete beam was experimentally tested and is widely used to confirm the validity of numerical methods of analysis [19]. The crack propagation in the beam is a mixture of opening mode I and sliding mode II. The beam is shown in Fig. 27. The following material data are assumed: $E = 35.0$ GPa, $\nu = 0.15$, $f_t = 0.0$ MPa. The relationship $\sigma = f(w)$ is of the form (85) where now $n = 4$ and $w_c = 0.167\,\text{mm}$, assuming fracture energy $G_F = 10\,\text{Nm/m}^2$. In the analysis the generalized fictitious crack model (GFCM) has been used [8].

The beam has been initially discretized using 945 triangle elements and 522 nodes, Fig. 28.

In Fig. 29 the discretisations of the beam in the process of crack growing for different coupling methods are shown. The process of analysis was steered with the crack mouth sliding displacement (CMSD).

In Figs. 30 and 31 the results of calculations in the form of equilibrium paths of the structure with a growing crack, reached with the help of standard and partition of unity computational models, are shown and compared with the experimental data. Additionally, in Fig. 31b the results of calculations using XFEM are also presented. In this example good agreements with experimental data for both models are seen. In case of analysis using XFEM the differences between experimental and numerical results are visible after passing a maximum load level.

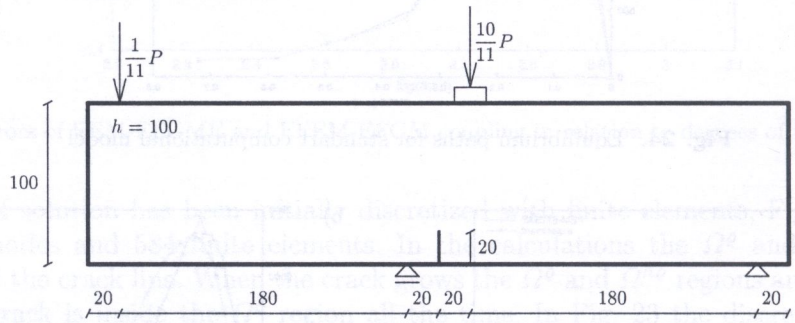

Fig. 27. Four point bent Iosipescu beam; measures in [mm]

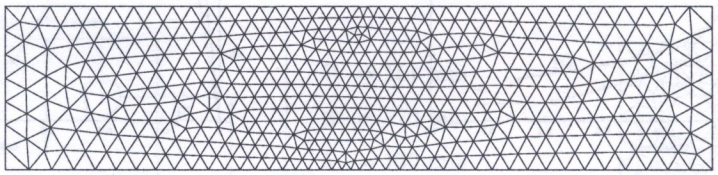

Fig. 28. The discretisation of Iosipescu beam with finite elements

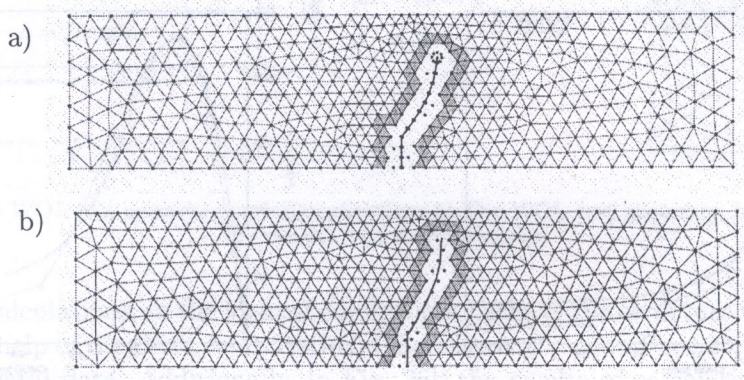

Fig. 29. Discretisation of Iosipescu beam for different coupling methods: a) FEM-EFGM, b) FEM-XEFGM

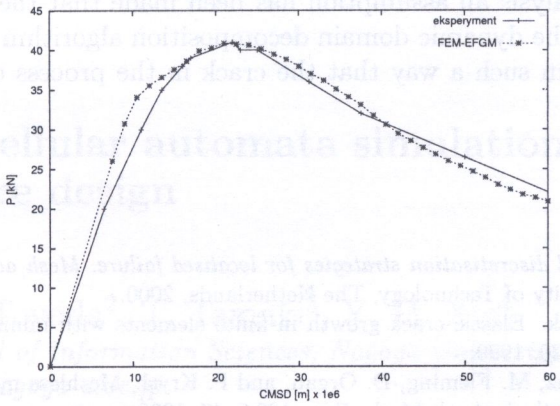

Fig. 30. Equilibruim paths for standart computational model

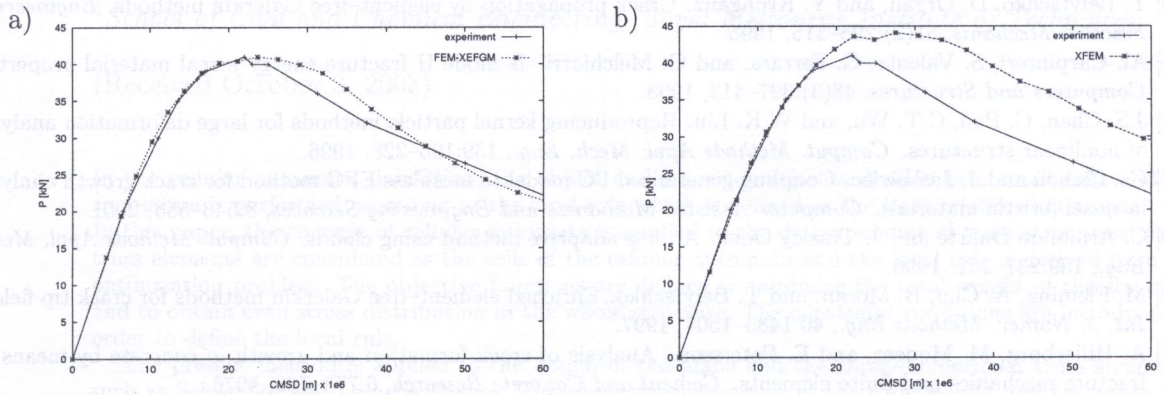

Fig. 31. Equilibruim paths for partition of unity computational model: a) FEM-XEFGM, b) XFEM

6. Conclusions

In the paper three computational models for crack growth analysis in quasi-brittle materials in plane stress state have been presented. These models have been worked out on the base of different methods of coupling the finite element method and the element free Galerkin method. The effectiveness of the methods of analysis have been improved by the algorithm of dynamic domain decomposition into Ω^h, Ω^{ϱ}, $\Omega^{h\varrho}$ parts. The usefulness of the methods in crack growth analysis has been confirmed in examples. In the authors' opinion the standard model and the partition of unity model are specially effective in crack growth analysis. Using the EFEM-EFGM coupling to the crack growth analysis gave unsatisfactory results, but on the other hand, for the analysis of L-shaped domain with singularity the method worked quite well. In addition, in case of using FEM-EFGM coupling the essential boundary conditions can be easily satisfied.

Detailed conclusions can be formulated as follows.

1. Coupling FE and EFG methods seems to be attractive in finding approximated solutions of engineering problems. Such approach applies the advantages of both methods and hides their drawbacks at the same time.
2. Consistency order of shape functions in the FEM-EFGM coupling can be improved in an arbitrary place inside Ω domain without changing the discretisation. In such a way the coupled methods can also be used as an adaptation technique of p type.
3. In the coupled methods special functions can be added to the approximation field in an arbitrary place of Ω domain. It means that in the case when the character of exact solution is globally or locally known, this information can be added to the approximated solution.

4. In the crack growth analysis an assumption has been made that the crack shape is not known *apriori*. It means that the dynamic domain decomposition algorithm updates automatically the domain decomposition in such a way that the crack in the process of growing is always inside Ω^{ϱ} or $\Omega^{h\varrho}$ part.

References

[1] H. Askes. *Advanced spatial discretisation strategies for localised failure. Mesh adaptivity and meshless methods.* Dissertation, Delft University of Technology, The Netherlands, 2000.

[2] T. Belytschko and T. Black. Elastic crack growth in finite elements with minimal remeshing. *Int. J. Numer. Methods Eng.*, 45(5):601–620, 1999.

[3] T. Belytschko, Y. Krongauz, M. Fleming, D. Organ, and P. Krysl. Meshless methods: an overview and recent developments. *Comput. Methods Appl. Mech. Eng.*, 139:3–47, 1996.

[4] T. Belytschko, D. Organ, and Y. Krongauz. A coupled finite element–free Galerkin method. *Computational Mechanics*, 17:186–195, 1995.

[5] T. Belytschko, D. Organ, and Y. Krongauz. Crack propagation by element–free Galerkin methods. *Engineering Fracture Mechanis*, 51(2):295–315, 1995.

[6] Al. Carpinteri, S. Valente, G. Ferrara, and G. Melchiorri. Is mode II fracture energy a real material property? *Computers and Structures*, 48(3):397–413, 1993.

[7] J.S. Chen, C. Pan, C.T. Wu, and W.K. Liu. Reproducing kernel particle methods for large deformation analysis of nonlinear structures. *Comput. Methods Appl. Mech. Eng.*, 139:195–228, 1996.

[8] Cz. Cichoń and J. Jaśkowiec. Coupling generalized FC model to meshless EFG method for crack growth analysis in quasi–brittle materials. *Computer Assisted Mechanics and Engineering Sciences*, 8:543–556, 2001.

[9] C. Armondo Duarte and J. Tinsley Oden. An *h–p* adaptive method using clouds. *Comput. Methods Appl. Mech. Eng.*, 139:237–262, 1996.

[10] M. Fleming, A. Chu, B. Moran, and T. Belytschko. Enriched element–free Galerkin methods for crack tip fields. *Int. J. Numer. Methods Eng.*, 40:1483–1504, 1997.

[11] A. Hillerborg, M. Modeer, and E. Petersson. Analysis of crack formation and growth in concrete by means of fracture mechanics and finite elements. *Cement and Concrete Research*, 6:773–782, 1976.

[12] A. Huerta and S. Fernández-Méndez. Enrichment and coupling of the finite element and meshless methods. *Int. J. Numer. Methods Eng.*, 48:1615–1636, 2000.

[13] Jan Jaśkowiec. *Integration of FEM and EFGM in two dimensional quasi–brittle crack growth analysis.* Dissertation (in Polish), Cracow University of Technology, Cracow, Poland, 2003.

[14] B.L. Karihaloo. *Fracture Mechanics and Structural Concrete.* Longman, 1997.

[15] J. Krok and J. Orkisz. A unified approach to the adaptive meshless FDM and FEM. In: *European Conference on Computational Mechanics*, Cracow Poland, June 26–29, 2001.

[16] S. Li and W.K. Liu. Meshfree and particle method and their applications. *Applied Mechanics*, 55:1–34, 2002.

[17] J.M. Melenk and I. Babuška. The partition of unity finite element method: Basic theory and applications. *Comput. Methods Appl. Mech. Eng.*, 139:289–314, 1996.

[18] E. Riks. On the numerical solution of snapping problems in the theory of elastic stability. Report, SUDAAR 401, Dep. Aeronautics and Astronautics, Stanford Univ. Calif. USA, 1970.

[19] J.N. Rreddy. *Applied Functional Analysis and Variational Methods in Engineering.* McGraw-Hiu Book Company, 1986.

[20] E. Schlangen. *Experimental and numerical analysis of fracture process in concrete.* Dissertation, Delft University of Technology, The Netherlands, 1993.

[21] T. Strouboulis, I. Babuška, and K. Copps. The design and analysis of the Generalized Finite Element Method. *Comput. Methods Appl. Mech. Eng.*, 181:43–69, 2000.

[22] M. van Gils. *Quasi-brittle fracture of ceramics.* Dissertation, Eindhoven University of Technology, 1997.

[23] G.A. Wempner. Discrete approximations related to nonlinear theories of solids. *Int. J. Solids. Stru*, 7:1581–1599, 1971.

[24] T. Zhu and S.N. Atluri. A modified collocation method and a penalty formulation for enforcing the essential boundary conditions in the element free Galerkin method. *Computational Mechanics*, 21:211–222, 1998.

[25] O.C. Zienkiewicz and R.L. Taylor. *The Finite Element Method.* Butterworth-Heinemann, fifth edition, 2000.